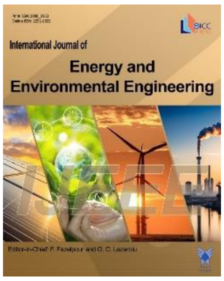

Volume 15, Issue 2, (2024) Article 7

International Journal
of
Energy and Environmental Engineering (IJEEE)

https://doi.org/10.57647/ijeee. 2024.1502.07

Solar Dish-Stirling Pump for Irrigation: Site Suitability and Performance Assessment

Tesfaye Abera Tesema[1,*], Venkata Ramayya Ancha[1], Endeshaw Alemu Bekele[2], Ephrem Assefa Feyissa[3]

[1] *Faculty of Mechanical Engineering, Jimma Institute of Technology, Jimma University, P.O. Box: 378, Jimma, Ethiopia*
[2] *Department of Astronautics, Electrical and Energetics Engineering DIAEE, Sapienza University of Rome, Rome, Italy*
[3] *Department of Mechanical Engineering, College of Engineering and Technology, Bule Hora University, P.O. Box: 144, Bule Hora, Ethiopia*

***Corresponding author:** tesfaye.aberra@ju.edu.et

Original Research

Abstract

The growing global population has intensified demand for water, food, and energy, straining fossil fuel reserves and accelerating climate change. Water scarcity, especially in developing countries, hinders sustainable development. Enhancing agricultural productivity through modern irrigation technologies is essential to reducing rain-fed dependence and ensuring food security. Solar energy offers a sustainable alternative for irrigation. This study evaluates a solar dish concentrator integrated with a Stirling engine-driven pump and conical cavity receiver. The system, featuring a 2.8 m aperture diameter and 0.4 m depth concentrator, was assessed across four Ethiopian sites (Ziway, Dangila, Itang, and Jigjiga) based on solar radiation, groundwater potential, and irrigation demand. Using a weighted matrix method, Ziway was identified as the most suitable site for detailed analysis. COMSOL Multiphysics simulation showed an average receiver surface temperature of 574 K. Results indicate that solar radiation variations significantly affect thermal output, dish efficiency, and flow rate. Under optimal conditions, concentrator and Stirling engine efficiencies reached 83.69% and 39.01%, with overall energy and exergy efficiencies of 23.38% and 25.07%. The system produced 132 W peak power and 24,240 L/day flow, confirming potential for sustainable irrigation and rural development.

Keywords: Solar irrigation; Sustainable agriculture; WEF nexus; Food security; Dish-Stirling engine

Cite this article: Tesema T. A., Ancha V. R., Bekele E. A., Feyissa E. A., Solar Dish-Stirling Pump for Irrigation: Site Suitability and Performance Assessment. Int. J. Energy Environ. Eng. 2024; 15(1) : 1-26 https://doi.org/10.57647/ijeee. 2024.1502.07

Highlights

- A pump, powered by a Solar Dish Stirling engine utilizing a conical cavity receiver, was proposed for use in the irrigation system.
- The Stirling engine achieved a maximum efficiency of 39.01% under the ideal regenerator condition
- The system's total energy and exergy efficiencies were found to be 23.38% and 25.07%, respectively

Nomenclature

A	Area	m^2
C	Concentration ratio	–
Cp	Specific heat capacity at constant pressure	J/ (kg-K)

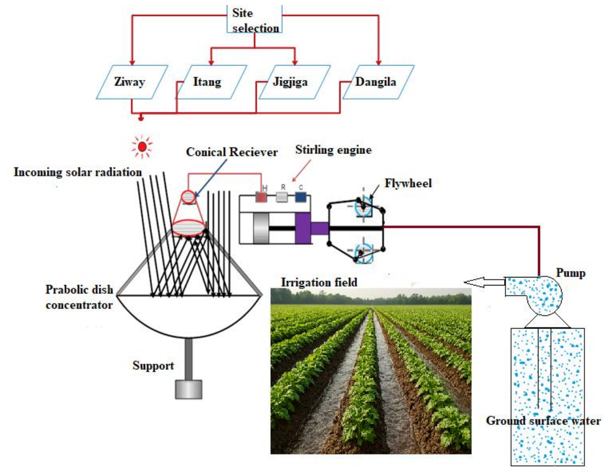

Cv	Specific heat capacity at constant pressure	J/ (kg- K)
f	focal length	m
g	Gravitational acceleration	m/s ^{2}
H	Total dynamic head	m
I	Solar irradiance	W/m^2
m_{air}	mass flow rate	Kg/s
PH	Hydraulic power	W
POUT	Output power	W
Pshaft	Shaft power	W
Q	flow rate	m^3/s
Q_{loss}	Total heat loss	W
Q_{abs}	Heat absorbed by the receiver	W
QU	Useful heat	W
T	Temperature	K, °C
VC	Compression space volume	cm^3
VDC	Compression space dead volume	cm^3
VDE	Expansion space dead volume	cm^3
VE	Expansion space	cm^3
VSD	Swept volume of a displacer	cm^3
VSP	Swept volume of the piston	cm^3
Vw	Wind velocity	m/s
W	Work done	J
Dca	Aperture's diameter	m

Abbreviation

ATA	Agricultural Transformation Agency
CC	Initial capital costs
COMSOL	Computational Multiphysics Simulation Software
CR	Compression Ratio
CR exp	Expansion Ratio
CROPWAT	Estimate crop water
CSP	Concentrated Solar Power
CWR	Crop water requirement
DNI	Direct normal irradiance
EES	Engineering Equation Solver
GDP	Gross Domestic Product
GIS	geographic information system
HTF	Heat Transfer Fluid
LCC	life cycle cost
MATLAB	Matrix laboratory
MOPSO	Multi-Objective Particle Swarm Optimization
NASA	National Aeronautics and Space Administration
NPV	net present value
NREL	The National Renewable Energy Laboratory
OECD	Organization for Economic Co-operation and Development
OM	Operation and maintenance costs
PDC	parabolic dish concentrator
PV	Photovoltaic
RC	Replacement cost
SOLTRACE	Solar Tracing Environment for Concentrated Solar Energy

List of symbols

A	Area(m^2)
C	Concentration ratio
A_{dish}	Collector area
Cp	Specific heat capacity at constant pressure (J/ (kg-K)
Cv	Specific heat capacity at constant (J/Kg-K)
Dca	Aperture's diameter(m)
Ex_{in}	Total energetic solar power input to the parabolic dish(W)
f	focal length (m)
g	Gravitational acceleration (m/s ^{2})
G_{sc}	Solar constant(W/m^2)
H	Total dynamic head(m)
I	Solar irradiance(w/m^2)
m_{air}	mass flow rate (Kg/s)
PH	Hydraulic power(W)
POUT	Output power(W)
P_{Shaft}	Shaft power(W)
Q	flow rate(m^3/s)
Q_{loss}	Thermal loss(W)
Q_{abs}	Power absorbed by receiver(W)
QU	Useful heat(W)
T	Temperature (K, °C)
VC	Compression space volume(cm^3)
VDC	Compression space dead volume(cm^3)
VDE	Expansion space dead volume(cm^3)
VE	Expansion space(cm^3)
VSD	Swept volume of a displacer(cm^3)
VSP	Swept volume of the piston(cm^3)
Vw	Wind velocity(m/s)
W	Work done(J)

Symbol

δ_s	Solar azimuthal angle(degree)

10.57647/ijeee. 2024.1502.07

n_{ex}	Total exergy efficiency
η_c	Concentrator efficiency (%)
η_{opt}	Optical efficiency (%)
K	Thermal conductivity(W/m.k)
α	Altitude angle(degree)
β	Coefficient of thermal expansion(1/K)
$\emptyset_r$	Rim angle(degree)
γ	Azimuthal angle(degree)
δ	Stefan Boltzmann constant(W/m^2K^4)
$\emptyset$	Local latitude(degree)
ε	Emissivity
ρ	Density of water($1000 kg/m^3$)
ω	Hour angle(degree)
θ	Acceptance angle(degree)

1. Introduction

Irrigation systems play a crucial role in ensuring food security and mitigating the impacts of drought and water scarcity. Solar-powered irrigation systems have emerged as a significant advancement in agricultural practices, [1] reducing carbon footprints and minimizing pollution associated with conventional irrigation methods [2]. Solar photovoltaic systems convert sunlight directly into electricity, which can power water pumps, while solar thermal systems use sunlight to heat water or generate steam. These technologies are particularly beneficial in agricultural contexts, where water and energy are critical resources [3]. The solar-powered irrigation system, water availability, and the moisture of the soil are the main pillars of the agricultural system. Irrigation water management must implement specific processes to improve food production using the 'more crop per drop' strategy [4]. The study also shows that improving irrigation management can be achieved through advanced technology and smart irrigation systems. Effective groundwater management is critical for future environmental, ecological, and social security and sustainability [5]. Solar-powered irrigation systems offer a sustainable alternative to conventional irrigation methods by harnessing solar energy for a reliable and cost-effective water delivery [6]. The energy-irrigation nexus has gained significant attention in regions rich in solar energy, highlighting the interdependence between water and energy resources. The transition to solar-powered irrigation from traditional technologies not only reduces greenhouse gas emissions but also offers substantial economic and operational benefits. This makes solar irrigation an environmentally responsible and economically viable solution for sustainable agriculture.

The economic and environmental potential of solar energy in irrigation is particularly notable in sub-Saharan Africa and South Asia, where conventional systems are often unreliable or costly. Recent research on the design and evaluation of solar-powered smart irrigation systems for sustainable urban agriculture underscores the transformative potential of such systems in enhancing food security, conserving water, reducing energy consumption, and mitigating carbon emissions in urban agriculture [7]. Solar energy reduces operational costs, improves agricultural productivity, and promotes environmental sustainability through automated and moisture-sensitive irrigation control [8]. Although the upfront capital costs of solar systems may be higher than those of diesel or electric alternatives, their long-term savings on operation and maintenance are significant [9]. Solar power systems have demonstrated significant emission reduction capabilities in agriculture and offer economic and social benefits, compelling a case for their broader adoption in global agriculture [10]. Among irrigation technologies, solar thermal technology offers several advantages over solar photovoltaic (PV) and diesel systems for irrigation, in terms of energy efficiency, cost-effectiveness, and environmental impact [11].

Solar-powered water irrigation systems have emerged as transformative, sustainable solutions for small-scale rural farming, offering low operational costs and reduced reliance on fossil fuels [12]. Solar thermal systems are generally cheaper to install compared to solar PV systems, which have higher startup costs despite lower ongoing operational expenses [13]. Solar thermal systems have a smaller carbon footprint compared to both solar PV and diesel systems, making them a more environmentally friendly option for irrigation [14]. Another study also confirmed that solar thermal systems offer a more economically viable solution for irrigation, reducing dependency on fuel subsidies and promoting green energy. The solar-powered Stirling engine has demonstrated the highest efficiency of converting solar energy into electrical power among concentrating solar power applications [15]. The solar thermal systems especially those employing parabolic dish Stirling engines have demonstrated superior energy conversion efficiency (12–25%), operational consistency, and suitability for off-grid irrigation applications compared to PV systems [12-17], and better performance at high temperatures, making them especially suitable for applications requiring consistent power supply [20,23]. Other studies also report that the solar dish Stirling system demonstrates a high solar-to-electric energy conversion efficiency, achieving a peak efficiency of up to 30% and an average efficiency ranging from 15% to 27%. Parabolic dish Stirling engines, in particular, are gaining attention due to their suitability for decentralized rural irrigation. These engines are capable of high energy conversion efficiencies, local manufacturability, and operation under varying heat sources, including solar, waste heat, and geothermal energy [21, 22, 24].

The solar dish–Stirling engine system represents a versatile and promising technology for cogeneration, enabling simultaneous electricity generation and freshwater production when integrated with adsorption or humidification–dehumidification processes [25]. Solar dish Stirling systems have been successfully integrated with desalination processes to simultaneously generate electricity, thermal energy, and freshwater.

Under specific operating conditions, such hybrid configurations have achieved overall efficiencies of up to 62.60%, significantly outperforming standalone systems [26]. Hybrid renewable energy systems have demonstrated superior stability and reliability compared to single-source systems, while operating at relatively low costs. A study conducted in Brack City, Libya, evaluated a hybrid system consisting of a 36,560 m^3 biomass digester producing 27 Mm^3 of biogas annually, a 1,230 kW Stirling generator, and a 6,006 m^2 parabolic dish solar concentrator (PDSC). The system contributes approximately 5,670,534 kWh of energy to the grid annually, with a peak load capacity of 1,230 kWh and a total coverage of 5,892,666 kWh [27]. The solar dish Stirling system is noted for its high solar-to-electricity conversion efficiency, reaching up to 23.40% in some configurations [28]. The widespread adoption of solar thermal-based irrigation systems faces challenges, including high initial capital costs, limited availability of spare parts, and a shortage of technical expertise, particularly in rural areas [29,30]. The challenge is compounded by the need for effective groundwater management and irrigation scheduling to avoid resource depletion and ensure sustainability. Despite these challenges, solar thermal technologies, when supported by proper design, policy, and training, hold promise for long-term sustainability in water-scarce agricultural areas [31,32]. Many studies have explored the design, simulation, and evaluation of solar thermal water pumping systems, with a specific focus on solar dish concentrators and Stirling engines [33]. The design of Dish/Stirling systems requires optimization of both the parabolic dish concentrator and the Stirling engine. Critical design parameters such as concentrator diameter, focal length, and rim angle play a major role in determining optical efficiency and the flux distribution on the receiver [34]. The thermal performance of Dish/Stirling systems is strongly affected by receiver operating temperature, direct normal irradiance, and surrounding environmental conditions. Increasing the concentrator diameter typically enhances both power output and overall efficiency [35]. An experimental investigation of a parabolic dish collector with a hemispherical cavity receiver using ethylene glycol–water mixtures revealed that solar irradiance peaks around midday, significantly influencing all thermal responses of the system [36]. Furthermore, hybrid configurations such as the integration of micro gas turbines can attain superior efficiency levels compared to conventional standalone systems [37].Dish/Stirling systems exhibit wide applicability, including use in distributed power generation, micro-scale cogeneration, and water desalination. The levelized cost of energy (LCOE) for such systems is reported to range between 0.115 and 0.256 USD/kWh, depending on the system scale and geographical location [38]. Optimal design and performance enhancement of thermodynamically balanced systems require an integrated approach that accounts for thermodynamic, economic, and environmental factors. Such optimization is essential for improving the efficiency and functionality of thermal systems, including thermoelectric refrigeration units, thermodynamic machines, and combined cooling, heating, and power systems [38]. These efforts have shown that incorporating two-axis tracking systems can significantly improve the performance of solar collectors, increasing their energy collection by 20%-30% [39]. The primary objective of this study is to conduct a comprehensive techno-economic feasibility analysis and performance evaluation of solar thermal-based irrigation systems for application in remote agricultural regions. The research aims specifically to assess the solar energy availability and the potential of water resources in the selected case study areas to determine the viability of sustainable irrigation. A critical part of the study involves the design and development of a concentrated solar power system, utilizing a Stirling engine to convert thermal energy into mechanical energy for water pumping. The research also undertakes detailed energy and exergy analysis to evaluate the thermodynamic performance and losses across the system.

2. Methodology and Materials

2.1. Description of the study areas

The research aims to assess the solar energy potential, the availability of water resources, and the irrigation demand of using a Stirling parabolic dish Stirling engine in four selected sites: Dangila, Ziway, Jigjiga, and Intag, as displayed in Figure 1. Based on solar potential, groundwater availability, and irrigation demand, each site will be analyzed and ranked. Subsequently, a score will be assigned to each site using a normalized matrix, and the site with the highest score will be selected as the case study for this research. Dangila is a town located in northwestern Ethiopia, within the Agew Awi Zone of the Amhara Region, approximately 475 km from Addis Ababa. It lies at a latitude of 11°16ºN, a longitude of 36°50ºE, and an elevation of 2,120 meters above sea level. Ziway, also known as Batu, is a town and district located within the East Shewa Zone of the Oromia Region, approximately 162 km from Addis Ababa. It is situated at a latitude of 7 ° 55' 59.99" N and a longitude of 38 ° 42' 59.99" E, with an elevation of 1,680 meters above sea level. Jijiga (Somali: Jigjiga) is a district in the Somali Region of Ethiopia, serving as the regional capital. Located 618 km from Addis Ababa, it sits at a latitude of 9 ° 22' 11" N and a longitude of 42 ° 49' 48" E, with an elevation of 1,935 meters above sea level. Itang is a district in the Gambela region of Ethiopia, located 816 km from the capital, Addis Ababa. The town is situated at a latitude of 8° 11 59" N and a longitude of 34° 16' 12" E, with an elevation of 647 meters above sea level.

2.2. Data collection and overall flow process of the work

The success of this study relies heavily on the accuracy and relevance of the data collected. To support the analysis, both **primary** and **secondary** data were

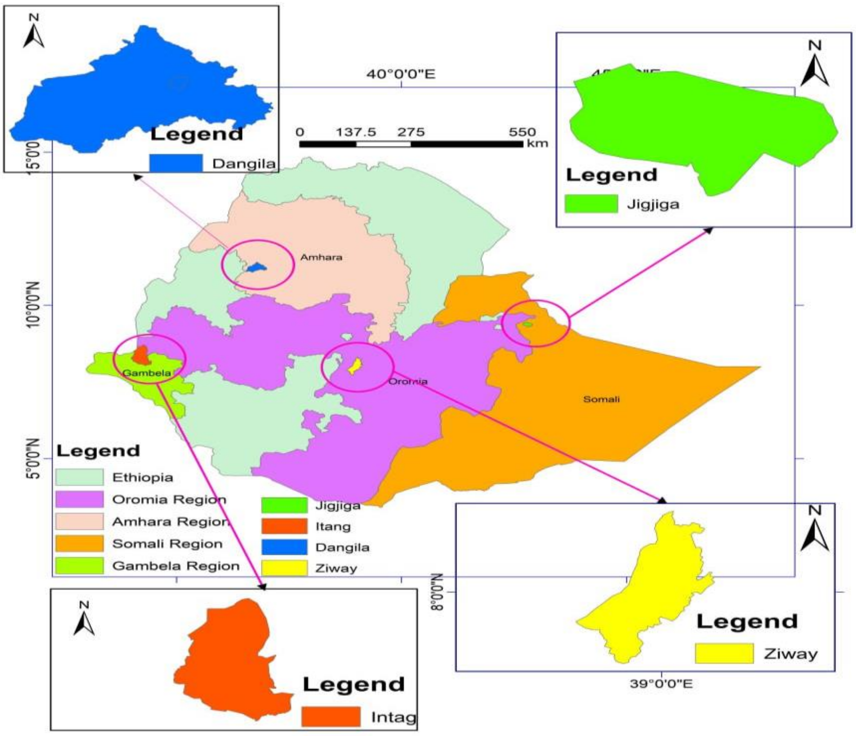

Figure 1. Map of the Study Areas

gathered and systematically utilized. The **primary data** were generated through simulation-based performance evaluations using specialized engineering software. The thermal behavior and optical performance of the solar concentrator were analyzed using the **Engineering Equation Solver (EES)**. **MATLAB** was applied to assess the ideal adiabatic efficiency of the Stirling engine under different operational conditions. **Sol Trace** was used to model and examine the solar flux distribution on the receiver surface, while **COMSOL Multiphysics** was employed to simulate the temperature distribution at the focal point of the parabolic concentrator. These simulations provided vital input for evaluating the technical aspects and operational behavior of the proposed solar thermal system. The **secondary data** were acquired from authoritative sources, including national institutions and published academic literature. Specifically, relevant information was collected from the **Ethiopian Ministry of Water and Energy**, the **Ministry of Agriculture**, and the **Ethiopian National Meteorology Agency (ENMA)**. Additional supporting data were sourced from books, scientific journals, and technical reports. Site-specific meteorological variables such as solar radiation and sunshine hours were estimated using the site's geographic coordinates (latitude and longitude) with the help of publicly accessible tools such as **NewLoc-Clim** and **NASA's Power Data Access** platform. The **Angstrom-Prescott model** was employed to estimate global solar radiation from sunshine duration data. The accuracy of these estimations was validated by comparing the results with datasets obtained from ENMA, NewLoc-Clim software, and NASA-based sources. By integrating simulated results from advanced software tools with validated secondary data from reliable institutions, the study ensures a rigorous and well-grounded assessment of the system's **economic feasibility** and performance for solar thermal-based irrigation applications. Figure 2 depicts the overall process flow and methods used in this work.

2.3. Description of the proposed system

The proposed system is composed of a dish concentrator, conical receiver, Stirling engine-driven pump, and fluid circulation component, as presented in Figure 3. Solar thermal systems absorb thermal energy from the sun via a solar concentrated surface. The parabolic dish concentrator concentrates the beam of solar radiation on the receiver at its focal point. Solar energy is directly transferred from the receiver's surface to the working fluid inside the absorber. Solar energy is directly transformed into thermal energy via a fluid or Stirling Cycle engine, which then converts the thermal energy into mechanical work. A Stirling engine produces mechanical work by utilizing cyclic compression and expansion of a working fluid (air) operating at different temperatures and enclosed in a fixed space. The air inside the cylinder will be expanded to produce work. The conversion of thermal energy into mechanical energy drives the piston's movement, which rotates the centrifugal pump's impeller. This mechanical energy is then transformed into hydraulic power, enabling the pump to move water at a specified head through the centrifugal pump.

2.4. Research gap

Unlike earlier studies that primarily focused on optimizing γ-type Stirling engines in dish-based CSP

10.57647/ijeee. 2024.1502.07

systems or assessing regenerator performance [40,41]. This work extends beyond technical optimization by integrating site-specific solar radiation potential, which is critical for accurate performance prediction and economic viability. Previous research examined dish-Stirling systems with thermoelectric generators but remained limited to cylindrical cavity receivers and overlooked the role of water resource availability.

An essential factor for irrigation applications. Moreover, most CSP optimization models have traditionally emphasized isolated thermal performance improvements, without adopting a multi-objective framework that simultaneously considers energy, exergy, and economic indicators under realistic operating conditions. The lack of such comprehensive thermodynamic analyses, together with the absence of performance data and design guidelines tailored to small-scale irrigation in regions like Ethiopia, has restricted localized implementation.To address these gaps, this study combines detailed solar radiation and groundwater resource assessments with the use of an underexplored conical cavity receiver, while conducting integrated energy, exergy, and thermo-economic analyses across diverse operating conditions. By explicitly linking technical optimization with economic feasibility for small-scale irrigation in rural Ethiopian settings, the research not only introduces innovative receiver geometry but also bridges the gap between theoretical system performance and practical application.

In doing so, it advances CSP–Stirling engine research beyond existing models and supports the deployment of solar thermal-based irrigation solutions in developing regions. Therefore, this study builds upon existing literature by evaluating the integration of solar thermal technology for irrigation within a framework that includes solar resource assessment, system design, energy and exergy analysis, and economic viability.

2.5. Justification and Comparative Evaluation of the Applied Calculation Model for Analyzing the Solar Dish Stirling Engine

The paper utilizes a mathematical model in MATLAB coupled with the EES package to analyze the performance of the proposed system due to its capability to handle complex calculations and simulate various operational conditions effectively. The calculation model in MATLAB was chosen for its ability to predict the dynamic behavior of the concentrator-receiver-Stirling engine system and quantify energy productivity under various conditions, allowing for a comprehensive analysis of performance improvement.

In general, the chosen calculation model for analyzing the performance of the Solar Dish Stirling engine integrates finite time thermodynamics and considers various factors affecting efficiency and output power. This model effectively captures the complexities of heat transfer, irreversibility, and system dynamics, making it suitable for optimizing performance.

Table 1. Summary of Research Gaps and Focus Areas

No	Focus area	Limitations/Gaps
1	Transient performance analysis of solar dish-Stirling systems with cylindrical cavities [42]	Did not address water resource potential or include energy and exergy analyses.
2	Impact of regenerators on Stirling engine performance [41]	Limited to engine optimization; no evaluation of conical receivers or water resource integration.
3	Optimization of CSP dish-powered γ-Stirling engines [40]	Did not examine systems with conical receivers or integrate solar radiation with water resource availability.
General Literature	Performance analysis and optimization of Stirling engines	Lack of focus on location-specific solar radiation, water resource assessment, and conical receivers.
Ethiopia-Specific Research	Adoption of parabolic dish-Stirling systems	Limited research on conical receivers, energy/exergy efficiencies, and small-scale irrigation systems

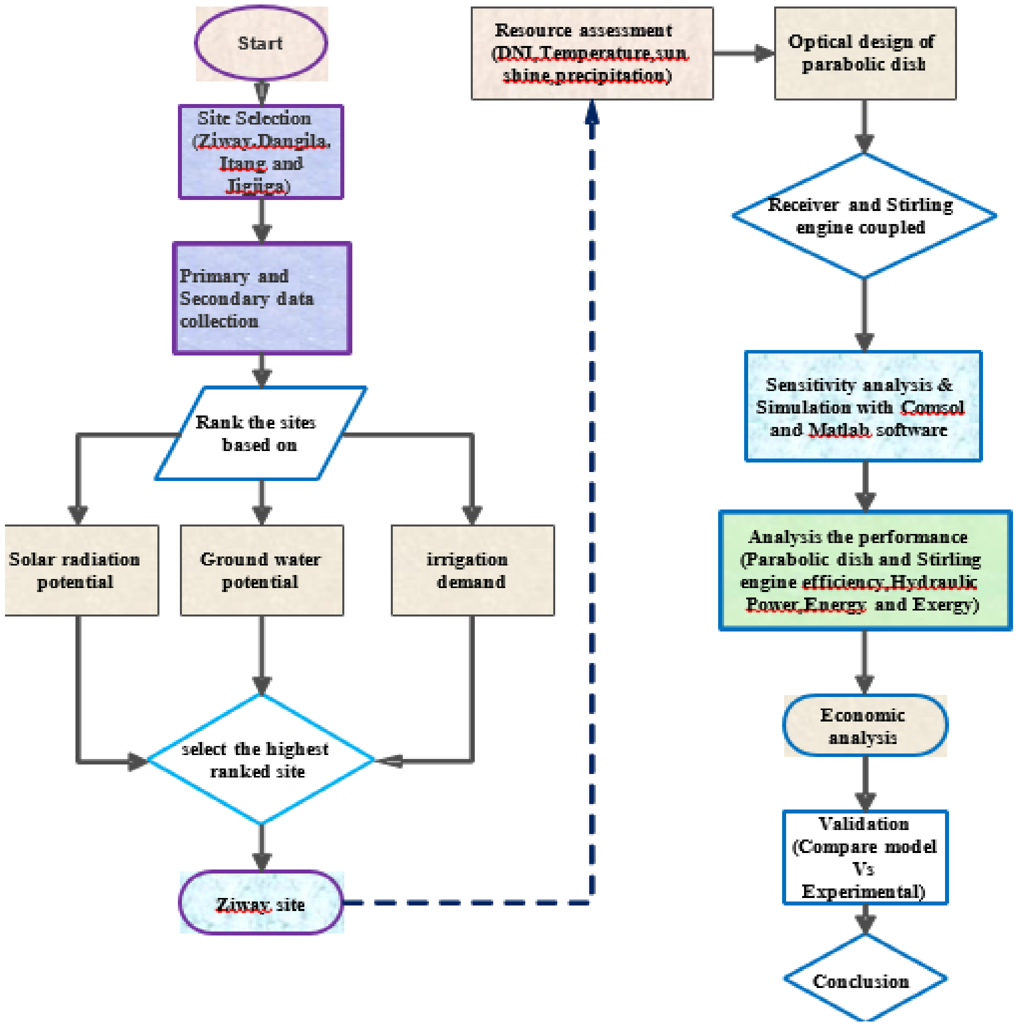

Figure 2. Research Design and Process Flow Chart

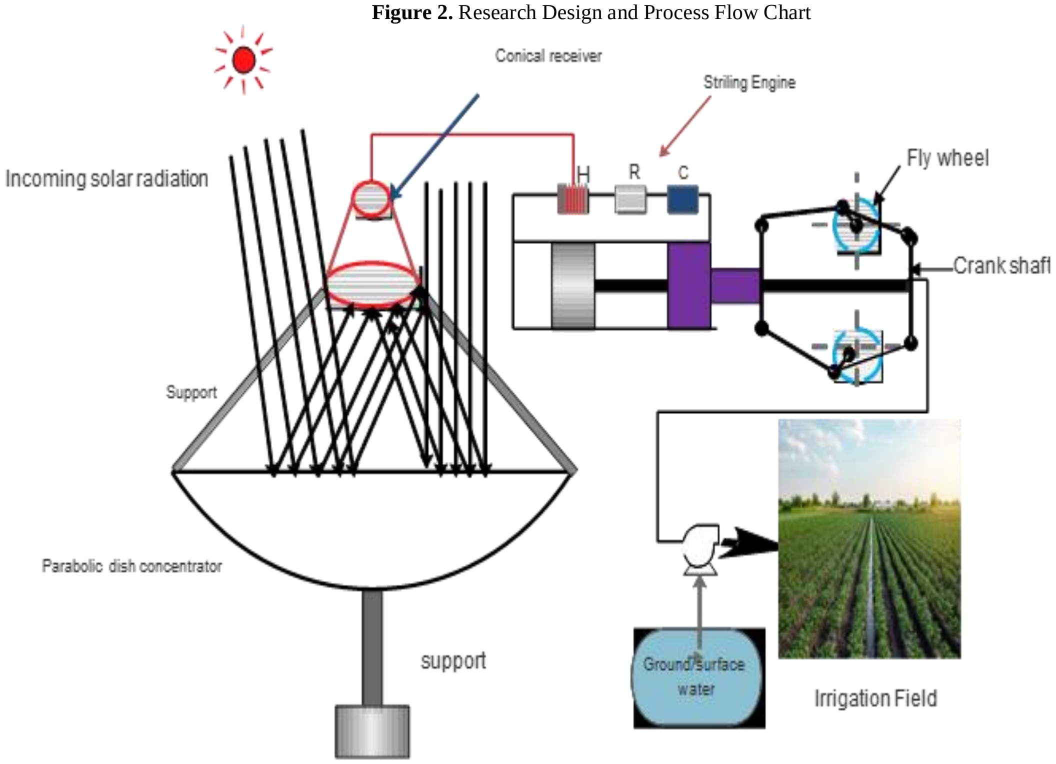

Figure 3. Operating Principle of the Suggested Model (Solar Dish Concentrator Combined with Stirling Engine.

Advantages of the Calculation Model

- **Comprehensive Representation:** The model incorporates both internal and external irreversibility, thereby improving the reliability of thermal efficiency and power output predictions
- **Optimization Potential:** It facilitates the optimization of critical parameters, such as absorber temperature, solar potential, to maximize power generation while accounting for heat transfer losses.
- **Dynamic Modeling:** Integration with MATLAB enables dynamic simulations, allowing performance of a Stirling engine assessment under varying operating conditions and supporting strategies for system enhancement.

Limitations of the Calculation Model

- **Computational Complexity:** The detailed formulation increases computational requirements and may complicate implementation
- **Simplifying Assumptions:** Dependence on assumptions, including idealized heat transfer conditions, may reduce accuracy in reflecting practical system behavior.

2.6. Solar Radiation Analysis

For the selected site, the solar radiation and sunshine duration were analyzed using meteorological data and mathematical estimation methods. Sunshine duration is a key factor in estimating solar radiation at a specific location. For a particular latitude and longitude, the sunlight data are obtained via the New_ LocClim estimator software. The New_ LocClim software, a free tool, enables the estimation of local climate conditions for sites without direct observational data. This software provides estimates for parameters such as temperature, precipitation, potential evapotranspiration, wind speed, water vapor pressure, and sunshine fraction or sunshine hours.

The **Angstrom–Prescott model** was applied to correlate solar radiation with sunshine duration, illustrated in Equations (1) and (2) below.

$$\bar{H}_h = \bar{H}_o\left(a + b\frac{\bar{n}}{\bar{N}}\right) \quad (1)$$

$$\bar{K}_T = \frac{\bar{H}_h}{\bar{H}_0} = \left(a + b\frac{\bar{n}}{\bar{N}}\right) \quad (2)$$

Where $\bar{H}_h and \bar{H}_o$ Represent the monthly average levels of horizontal terrestrial and horizontal extra-terrestrial radiation, respectively. The standard Angstrom coefficients recommended by the Food and Agriculture Organization are (a = 0.25 and b = 0.5) [43]. Maximum possible sunshine duration depends on the latitude of the site and the solar declination angle, and can be computed by the equation below [44].

$$\bar{N} = {}^{2}/_{15}\cos^{-1}[-tan(\emptyset)tan(\delta)] \quad (3)$$

Where $\bar{N}$,$\emptyset$ and δ represent the maximum possible sunshine duration, local latitude, and declination angle, respectively. The declination angle is calculated using the equation below [48].

$$\delta = 23.45sin\left[\frac{360}{365}(284 + N)\right] \quad (4)$$

Where N represents the number of days in a year.
The monthly average radiation outside the atmosphere ($\bar{H}_0$) can be calculated using the Klein relationship. [45] This represents the solar radiation received on a horizontal surface at the top of the Earth's atmosphere and can be estimated using Equation 5.

$$\bar{H}_0 = \left[\frac{24 * 3600}{\pi}\ G_{sc}\right] * \left[\left(1 + 0.033\cos\left(\frac{360N}{365}\right)\right)\right] * \left[\cos\phi\ \cos s\delta\ \sin\omega_s + \frac{\pi}{180}\omega_s \sin\phi\ \sin\delta\right] \quad (5)$$

G_{sc} is a solar constant (1367 $\frac{W}{m^2}$

$$\omega_s = \cos^{-1}(-tan(\emptyset)xtan(\sigma)) \quad (6)$$

Where ω_s represents the Sunset hour angle.

2.7. Water Resource Assessment

Water resource assessment was conducted to evaluate the groundwater availability and irrigation suitability of the selected case study areas using **ArcGIS spatial analysis** and secondary data obtained from hydrological and geological references ([56–67]).

2.8. Rainfall potential of the study areas

Rainfall and precipitation patterns in Sub-Saharan Africa exhibit significant variability influenced by geographic, climatic, and anthropogenic factors. The region experiences diverse rainfall regimes, with notable differences across various areas, such as the Sahel, East Africa, and Central Africa. Understanding these patterns is crucial for water resource management and addressing future water stress [57]. Rainfall in Ethiopia is highly variable, with a coefficient of variation ranging from 9% to 69% depending on the season and region [58]. The estimation of rainfall and effective rainfall was performed depending on CROPWAT and New locClim software using the site-local latitude and longitude.

2.9. Concentrator Efficiency

The efficiency of the dish concentrator is defined as the ratio of the useful output energy to the input energy, as shown in Equation 11.

$$\eta_C = \frac{Q_u}{I * A_{dish}} \tag{11}$$

Where η_C, A_{dish}, Q_uI represent the efficiency of the concentrator, collector area, and useful energy, respectively.

2.10. Performance of the receiver

The receiver's efficiency is defined as the ratio of the thermal heat collected by the working fluid (Q_u) to the total energy received within the concentrator's aperture (Q_{abs}) as below [59].

$$\eta_R = \frac{Q_u}{Q_{abs}} \tag{12}$$

Where:
η_R is the efficiency of the receiver.
Q_{abs} is the power absorbed by the receiver
The absorbed power is calculated as equation below [60]

$$Q_{abs} = I * A\_dish * \eta_{opt} \tag{13}$$

The thermal input energy to the Stirling engine (Q_{SE}) and the energetic power input (Q_{in}) are calculated using Equations (14) and (15), respectively [61].

$$Q_{SE} = \eta_C * \eta_R * I * A_{dish} * n_{opt} \tag{14}$$

$$Q_{abs} = I * A_{dish} * n_{opt} \tag{15}$$

The outlet temperature of the system is calculated as Equation below [42].

$$Q_{abs} - Q_{loss} = \dot{m} * c_p(T_{out} - T_{in})$$

Where Q_{in} is the absorbed solar energy, Q_{loss} is the thermal loss, $\dot{m}$ is the mass flow rate, c_p is the specific heat, T_{in}, the inlet, and T_{out} Outlet temperatures.
The system's overall power output is computed as in the equation below [62].

$$P\_SE = I * A_{dish} * n_{total}$$

Where P_SE and n_{total} represent the total power output and the system's total efficiency, respectively.
The total energetic solar power input to the parabolic dish and the total exergy efficiency are calculated using Equations (18) and (19), respectively.

$$E_{x\,in} = Q_{abs}\left[1 - \frac{4}{3}\left(\frac{T_a}{T_s}\right) + \frac{1}{3}\left(\frac{T_a}{T_s}\right)^4\right]$$

Where:
$E_{x\,in}$ =$E_{x\,in}$
T_a = ambient temperature (K).
T_s = effective temperature of the sun (~5600 K),

Therefore, the total exergy efficiency (n_{ex}) of the system is calculated as:

$$n_{ex} = P\_SE/E_{x\,in}$$

2.11. Power and Flow Rate of Each Site

In this section, the March season, which is the peak irrigation period for each site, is considered, and the hydraulic power and flow rate required to irrigate a hectare of land with a single system are calculated.

In a sub-arid climate, the average crop water requirement is 26.66 mm per week. Assuming an irrigation efficiency of 80 percent and a system operation of eight hours per day, six days a week, the amount of land area to be irrigated is estimated as follows:
Total operational time per week;

$$T_{week} = \frac{8hr}{day} * \frac{6day}{week} = 48\left(\frac{hr}{week}\right)$$

The total water volume pumped in the week is calculated using Equation (8) [63].

$$V_{pump} = Q_{pump} * T_{week}$$

Effective water available for irrigation;
$V_{eff} = Vpump * \eta$
Crop water requirement (CWR):
CWR=0.02666m/week
The irrigated area, based on the effective volume and crop water requirement, is calculated using Equation (22)[64].

$$A = \frac{V_{eff}}{CWR}$$

Where A represents the irrigated hectare of land from a single system.
The required hydraulic power to irrigate the proposed irrigation land area can be calculated below [65].

$$P_p = \frac{A_P P_S}{A_S}$$

Where: $P_p$represents the hydraulic power needed for the projection, A_P is the area specified for the projection, A_s is the irrigated area for a single-unit system, and P_S is the hydraulic power of a unit system. The total flow rate required to irrigate a specific number of hectares of land is calculated as below [66].
Q_required(m3/hr) =net irrigation(m/week) *Area in(m^2)/(H*D*E)

Where H, D, and E represent the static head, hours per day, and irrigation efficiency, respectively.
By considering the centrifugal pump efficiency as 85% and the average solar radiation of each site during the irrigation season in March, the inner surface temperature of the receiver was analyzed using **Sol Trace and**

COMSOL Multiphysics, while MATLAB was employed to calculate the hydraulic power and flow rate.

2.12. Estimation of Total Flow Rate Required (Q)

The flow rate needed for irrigation is calculated as in the equation below [66].

$$Q = \frac{N_{et\,app} * A}{H * D * E}$$

Where;
Q = Total flow rate required (m³/hr)
NetApp = Net irrigation depth needed per week (mm)
A = Total area to be irrigated (hectare)
H = Total hours available to operate the system per day
D = Total days to operate each week
E = Efficiency of the irrigation system (as a decimal)
Calculate the Hydraulic Power (P_H)
The estimate of hydraulic power required by the pump is calculated as equation below.

$$P_H = \frac{\rho g Q H_T}{3600}$$

Where:

ρ = Density of water (1000 kg/m³)
g = Gravitational acceleration (9.81 m/s²)
Q = Flow rate (m³/hr)
T_H = Total dynamic head (m)
The shaft power required and the amount of water pumped daily are determined using Equations (26) and (27), respectively [76].

$$P_H = \eta_p * P_{shaft}$$

Where P_H, η_p, and P_{shaft} are the hydraulic power, pump efficiency, and shaft power, respectively.

$$Q = \frac{V}{t_s}$$

Where:
Q Daily Water Pumped
V = Daily water requirement (m³/day)
t_s= Average number of sunny hours per day

2.13. Life-Cycle Cost Analysis of Parabolic Dish Stirling, PV, and Diesel-Based Irrigation Systems

Compared to traditional irrigation, the solar irrigation system offers a visually appealing and affordable method of water supply. To ascertain the project's economic viability, economic metrics such as net present value (NPV), internal rate of return (IRR), and simple payback period were examined.

An equal and practical comparison of solar and conventional water pumping technology is made possible by life cycle cost (LCC) analysis [67].

LCC for Stirling pumps and parabolic dish concentrated solar power includes startup, operating, maintenance, and replacement expenses. Manufacturing the concentrator, receiver, stirring engine, cooling system, controlling system, transporting the component to the site preparation, and installing the system constitute the system's initial capital investment. Labor, material, and maintenance expenditures are all included in operation and maintenance costs. The cost of replacing the battery is included in the replacement cost, which varies according to how many replacements are required during the plant's lifetime.

The present value is given in terms of a future cash amount occurring at the end of year *n* and the discount rate (*d*), while the uniform present value, present worth factors, and life cycle cost are computed using Equations (28), (29), (30) and (31), respectively, as shown below [38].

$$PV = F_n \frac{1}{(1+d)^n}$$

Uniform present value also calculates the present value of a series of equal cash amounts (Ao) that repeat annually over "n" years and a discount rate(d).

$$PV = A_o * \frac{(1+d)^n - 1}{d * (1+d)^n}$$

The present worth factor is computed as;

$$P_R = \left(\frac{1+i}{1+d}\right)^n$$

Where "i" is an inflation rate and "d" is a discount rate. LCC is estimated by adding the present worth of all costs of the components over the lifespan of the project. It is given as;

$$\mathrm{LCC} = \mathrm{CC} + \mathrm{OM} + \mathrm{RC} + \mathrm{FC}$$

Where CC is initial capital costs, OM is operation and maintenance costs, RC is replacement cost, and FC is fuel cost.

The annual fuel cost for the diesel generator is calculated using Equation (32) presented below.

$$\text{Fuel consumption} = \text{Specific fuel consumption} \times \text{Total operating hours} \times \text{Fuel rate}$$

3. Design of solar Dish concentrator and Thermal Stirling Pump

3.1. Design of Solar Dish Concentrator

The design of a parabolic dish is affected by many parameters that include the material of the reflector concentrators, the diameter of the parabolic dish concentrator, the size of the concentrator's aperture area, the focal length of the parabolic dish, the diameter of the focal point, the size of the receiver's aperture area, the geometric or area concentration ratio, and the rim angle. For the analysis, a dish concentrator with a 2.8 m aperture diameter and 0.4m depth of 0.4 m is considered

[42]. The design parameters of the dish concentrator and receiver are estimated, and their values are summarized in Tables 3 and 4.

3.1.1 Justification of Using a Conical Cavity Receiver

The conical cavity receiver is selected for its superior thermal and optical performance in dish–Stirling systems. Its geometry allows for effective concentration of reflected solar radiation onto a smaller absorber surface, resulting in higher energy density and uniform temperature distribution. In solar thermal applications, conical cavity receivers are integral to improving the efficiency of parabolic dish collectors. These receivers absorb and distribute heat effectively, with simulations showing that factors like pitch and fluid flow velocity can enhance heat transfer performance [28]. Experimental studies confirm that conical cavity receivers achieve higher thermal and energetic performance compared to other geometries, with minimal pressure drop [68]. The study focuses on the **optical efficiency** and **flux distribution** of three different receiver geometries: cylindrical, conical, and spherical. The **conical-shaped receiver** received and absorbed a higher amount of reflected flux energy compared to the other geometries. The **optical efficiencies** were found to be **75.3%, 70.1%, and 71.5%** for the conical, spherical, and cylindrical receivers, respectively [69].

Table 2. Potential of Groundwater Resources in the Selected Case Study Areas

Case studies	Recharge Potential	Irrigation Suitability	Justification	Reference
Ziway	2.1% excellent, 52.9% good, 43.4% moderate recharge zones	Moderately suitable (requires water quality monitoring) Approximately 83.4% of the area is suitable for surface irrigation. Groundwater Potential: High to Moderate	The area has good recharge potential, especially in the highlands, making groundwater availability feasible. Alluvial deposits near Lake Ziway and rivers (Meki River) are highly permeable and rechargeable, providing significant groundwater storage. The fractured basalts in the Rift Valley act as productive aquifers. Challenges include salinization risk near the lake due to evaporative concentration.	[46] [47] [48]
Dangila	An annual recharge of 17,717,690 m³, representing 15.8% of annual rainfall	Highly suitable (especially for shallow well irrigation) Groundwater Potential: High to Moderate	The current use of groundwater for irrigation is sustainable. Dangila has abundant recharge from rainfall and favorable shallow aquifers. Fractured basalts in the highlands have shallow, moderate permeability but are extensive and offer regional groundwater storage. Alluvial valleys (tributaries of the Blue Nile) have high-yield aquifers. Steep topography may limit groundwater accumulation in upland areas.	[49] [50]

Table 2. Potential of Groundwater Resources in the Selected Case Study Areas(continued)

Case studies	Recharge Potential	Irrigation Suitability	Justification	Reference
Itang	has an estimated groundwater potential ranging from 2.5 to 47 billion cubic meters, with a mean annual recharge of approximately 39.1 mm	The area has been mapped for potential irrigation use Groundwater Potential: Very High	Alluvial aquifers along the Baro River and its tributaries are highly permeable and extensively recharged by seasonal flooding. Flat topography and clay layers in some areas may create semi-confined aquifers with artesian potential. Risk of contamination from surface water during floods Has the most abundant water resource	[51] [52]
Jigjiga	The annual average rainfall is about 250 mm. The estimated monthly average recharge varies from 2.78 to 164 mm	Groundwater Potential: Low to Moderate	Sedimentary aquifers (Adigrat Sandstone) have moderate storage but are limited. Groundwater is often deep and localized in wadi systems (seasonal riverbeds). High evaporation rates and overextraction risk in this drought-prone region. Brackish water may occur due to low recharge and mineral dissolution in sedimentary layers. Irregular rainfall and high evapotranspiration affect groundwater recharge and availability.	[53] [54] [55] [56]

Table 3. Geometric Parameters of the Parabolic Dish Concentrator

Parameters	Unit	Numerical values
Aperture diameter	M	2.8
Focal length	M	1.225
Depth of the concentrator	M	0.4
Collector aperture area	m^2	6.158
Rim angle	Degree	59.49
f/d ratio	-	3.063
Arch length	M	4.067
Concentration ratio	-	1346
Rim radius	M	1.625

Table 4. . Specifications of the cavity receiver

Parameters	Unit	Numeric al values
The aperture's diameter (Dca)	m	0.052
Length of the receiver (l)	m	0.03
The inner Radius of the absorber	m	0.016
The outer radius of an absorber	m	0.026
Radius of Insulation	m	0.03
The top radius of the receiver	m	0.006

10.57647/ijeee. 2024.1502.07

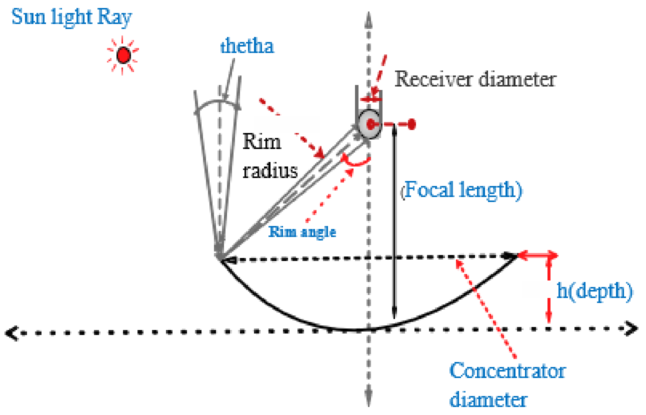

Figure 4. Schematic Diagram of the Parabolic Dish Concentration Geometry

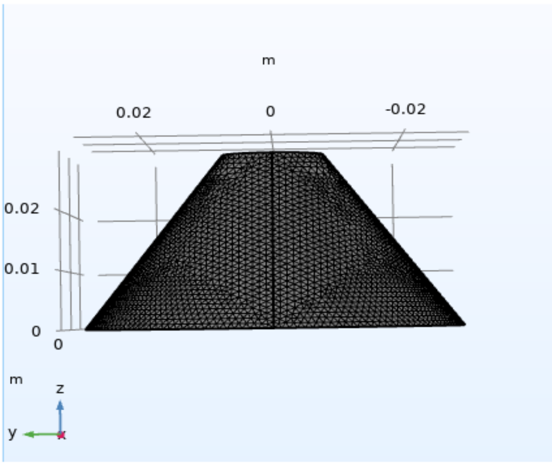

Figure 5. The geometry of the conical cavity receiver

Table 5. Design specification of the Stirling engine

Parameters		Value	Unit
Engine type		Beta	-
Working fluid		Air	-
	Diameter	72	mm
Displacer	Stroke length	34	mm
	The swept volume of a displacer	150	cm^3
	Diameter	65	mm
Power piston	Stroke length	32	mm
	The swept volume of the piston	80	cm^3
Regenerator	Diameter	42	mm
	Height	26	mm
	Porosity	79	%
	Void volume	36.02	cm^3
Heater	Diameter	22	mm
	Length	225	mm
	Void volume	85.53	cm^3
Cooler	Diameter	22	mm
	Length	55	mm
	Void volume	20.91	cm^3
Phase angle		90	Degree
Mean pressure		1	MPa
Expansion gas temperature		574	K
Compression gas temperature		300	K
Engine speed		450	RPM

3.2. Design Thermal Stirling Pump

The regenerative heat exchanger and the closed-cycle regenerative engine were created by Robert Stirling. He claims that the efficiency of the dish concentrator is defined as the ratio of the useful output energy to the input energy. The engine is called a stirring engine. To produce power, it works by compressing and expanding the working gas at various temperatures. The Stirling engine has better thermal efficiency than other engines. Theoretically, its thermal efficiency is close to that of the Carnot cycle. The expansion space, compression space, regenerator, heater, and cooler are the primary parts of the Stirling engine. Furthermore, in its optimum condition, the thermodynamic cycle of this engine consists of two constant volume operations (heat recovery in the regenerator) and two isothermal processes (isothermal expansion and compression)[70]. The Stirling engine operates using heat sources such as biomass, solar energy, and combustible materials. It offers several advantages, including quiet operation, zero emissions, and environmental sustainability[71].

4. Results and Discussion

4.1. Site Selection and Ranking

The site selection was carried out by comparing the potential of solar radiation, groundwater resources, and irrigation demand for each site. Appropriate weights were assigned to all criteria, and a matrix method was used to evaluate and rank the sites. The site with the highest overall score was selected and considered the study area. Based on Table 8, the normalized equation was applied, and weights were assigned to each criterion: 0.4 for solar radiation, 0.3 for groundwater availability, and 0.2 for irrigation demand. The data were analyzed using MATLAB matrix code. The sites Ziway, Itang, Jigjiga, and Dangila received scores of 0.75, 0.466, 0.375, and 0.2833, respectively, in descending order. Therefore, Ziway ranks highest among all the sites and is selected as the case study for this research. Accordingly, the subsequent analysis is carried out for the Ziway site.

4.2. Rainfall potential of the study areas

According to the data illustrated in Figure 6, Dangila receives significantly more rainfall compared to the other study areas, particularly during June, July, and August. In contrast, Jigjiga experiences much lower rainfall during these same months. The consistently high rainfall in Dangila throughout this period indicates a long and intense rainy season. However, from November to February, Dangila receives very little precipitation, marking a distinct dry season. The seasons with higher rainfall indicate that the site requires less irrigation. Thus, irrigation demand and rainfall are inversely proportional. Seasonal rainfall patterns show that periods of higher precipitation reduce the need for supplemental irrigation, whereas lower rainfall increases irrigation requirements. This demonstrates a clear inverse relationship between rainfall availability and irrigation demand. In general, among the four sites, Ziway exhibits the highest average irrigation requirement across the seasons.

4.3. Estimation of Monthly Average Daily Precipitation and Evapotranspiration

Irrigation systems are required when potential evapotranspiration exceeds actual precipitation, except during the wet season, when excessive rainfall eliminates the need for pumping. Therefore, irrigation becomes necessary only when crop water requirements (evapotranspiration) are greater than available rainfall (precipitation). According to Figure 7, Dangila receives the highest total precipitation among the selected areas, indicating a lower irrigation demand. On the contrary, Ziway has the lowest monthly average daily precipitation, suggesting that it has a higher irrigation demand due to insufficient and less frequent rainfall.

Based on the monthly average evapotranspiration data of the selected areas, the **Itang s**ite exhibits a higher irrigation demand during **January to March** and **November to December, as displayed in** Figure 8. In contrast, **Dangila** shows a lower irrigation demand during the period from **April to July.** The irrigation period for **Jigjiga** and **Ziway** is suitable from **October to the end of June**, while for **Itang** and **Dangila**, the suitable period spans from **October to the end of May**. Therefore, considering both rainfall and the precipitation-to-evapotranspiration ratio, **Ziway** has the highest irrigation demand, followed by **Jigjiga, Itang**, and **Dangila**, in descending order.

4.4. Solar energy potential of the study areas

According to sunshine hour data obtained from the New_ LocClim software and presented in Figure 9, the daylight duration at the Dangila site shows a sharp decline from April to July, followed by a noticeable increase from September to October. The maximum duration of sunshine at this site was recorded in February, reaching 8.9 hours per day, while the minimum was observed in August, with 2.14 hours per day. However, the average monthly duration of sunshine at the four selected sites, Ziway, Jigjiga, Dangila, and Itang, was found to be 7.5, 7.1, 6.6, and 6.0 hours per day, respectively, in descending order. This indicates that the Ziway site has the longest duration of sunshine among the selected locations.

Based on sunshine hour data obtained from the NewLocClim software and analyzed using the CROPWAT software, the highest monthly average solar radiation was recorded at the Ziway site, reaching 20 MJ/m²/day. On the contrary, the Itang site showed the lowest value, with an average of 17.7 MJ/m²/day. Other sites, Jigjiga and Dangila, received 19.3 MJ/m²/day and 18.4 MJ/m²/day, respectively.

10.57647/ijeee. 2024.1502.07

These variations in solar radiation at the selected sites are illustrated in Figure 10.

On the other hand, the Angstrom equation was one of the earliest methods used to estimate solar irradiance on a horizontal surface. Based on estimates from the Angstrom equation, the Ziway site receives the highest average solar radiation among the studied locations, as shown in Figures 10 and 11. Despite this, its solar radiation reaches a minimum during July and August, with recorded values of 11.65 MJ/m²/day and 12.02 MJ/m²/day, respectively.

The Dangila site follows a similar pattern, also showing its lowest radiation levels in the same months, 11.48 MJ/m²/day in July and 11.87 MJ/m²/day in August. On the contrary, the Itang site records the lowest average monthly global solar radiation. Dangila ranks third in terms of monthly average solar radiation, after the Ziway and Jigjiga sites.

Table 6. Selection of the Case Study Based on Multi-Criteria Analysis

Case study areas	Solar radiation	Water Resource Potential	Irrigation Season Demand
Dangila	3rd	4th	4th
Itang	4th	1st	3rd
Jigjiga	2nd	3rd	2nd
Ziway	1st	2nd	1st

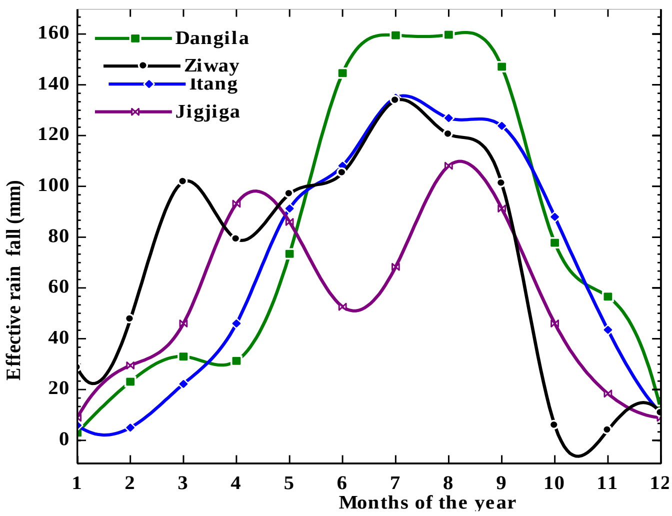

Figure 6. Effective Rainfall of Study Areas

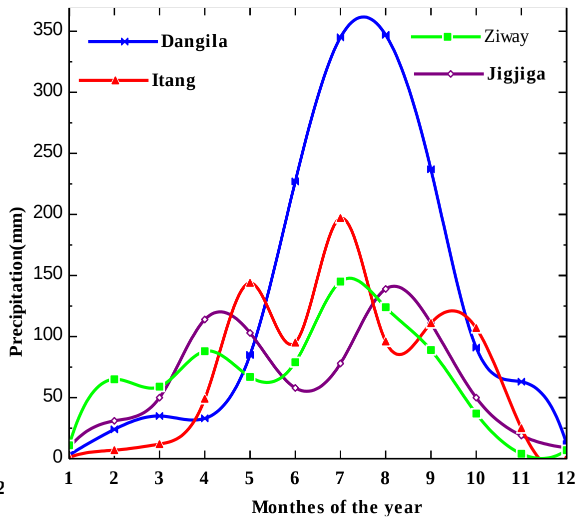

Figure 7. Monthly Average Daily Precipitation of Selected Areas

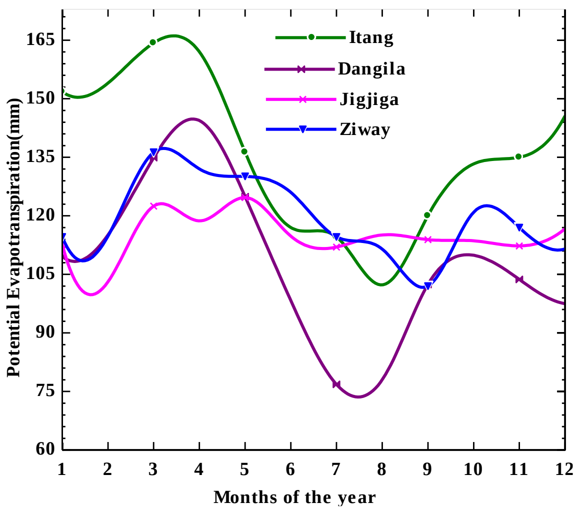

Figure 8. Monthly Average Evapotranspiration of Selected Areas

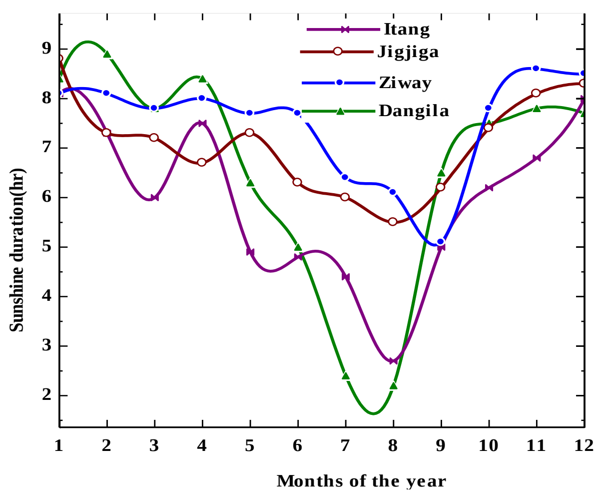

Figure 9. Monthly Average Daily Sunshine Duration

10.57647/ijeee. 2024.1502.07

4.5. Assessment of Hydraulic Power and Water Discharge for the Selected Sites During March

At the average solar radiation, if the pump operates for six hours per day in March, it can pump a minimum of 17,940 liters per day at Itang and a maximum of 19,380 liters per day at Ziway. The pump's flow rates at Dangila and Jigjiga are 18,000 L/day and 18,600 L/day, respectively. Thus, based on Equation 9, a single system at Ziway, Dangila, Itang, and Jigjiga can irrigate 0.466, 0.45, 0.42, and 0.43 hectares of land, respectively.

4.6. Estimation of Monthly Average Hourly Solar Radiation of Ziway Site

As illustrated in Figure 14, the average hourly solar radiation gradually rises after sunrise, reaches its peak around midday, and then declines toward sunset. In March, the peak beam solar radiation at noon reaches approximately 1000 W/m², whereas in October, it is slightly lower, peaking around **900 W/m²**. The system operates at full capacity in March, allowing the Stirling pump to meet the higher water demand of the irrigation system during this month.

4.7. Effect of solar radiation on flux intensity at the absorber of the concentrator

By considering the **average solar radiation** of the selected site as **700 W/m²** and importing this value into the **SolTrace software**, the simulation results indicate that the **power per ray** is **0.423W**, while the **total power** of the traced rays is **3950.97 W**.

According to the figure below, **10,000 beams** were subjected to the optical analysis. The simulation results show that **9,208 rays**, corresponding to **92.08%** of the emitted beams, successfully reached the **receiver surface**.

The **Sol Trace software** simulated an **average heat flux** of **1.5576 × 10⁶ W/m²**, as shown in Figure 16. This average heat flux was then **imported into COMSOL** to analyze the **inner surface temperature** of the receiver.

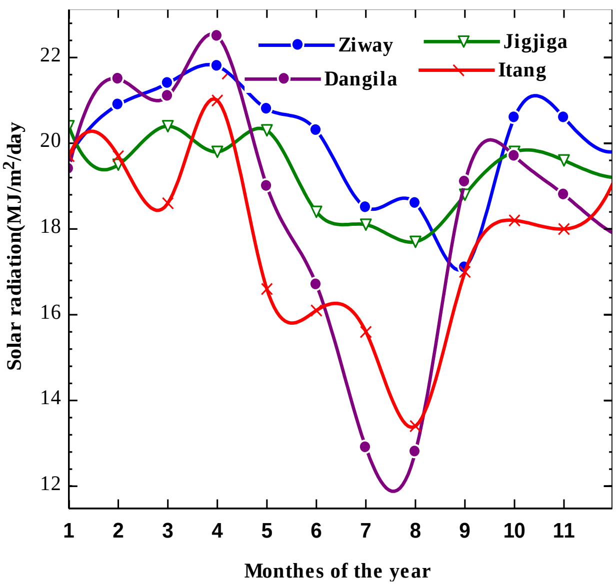

Figure 10. Monthly Solar Radiation of Selected Areas

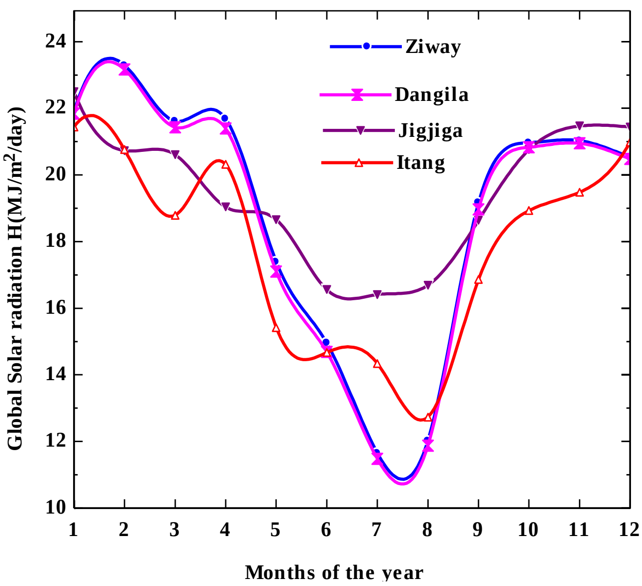

Figure 11. Monthly Global Solar Radiation of Selected Areas

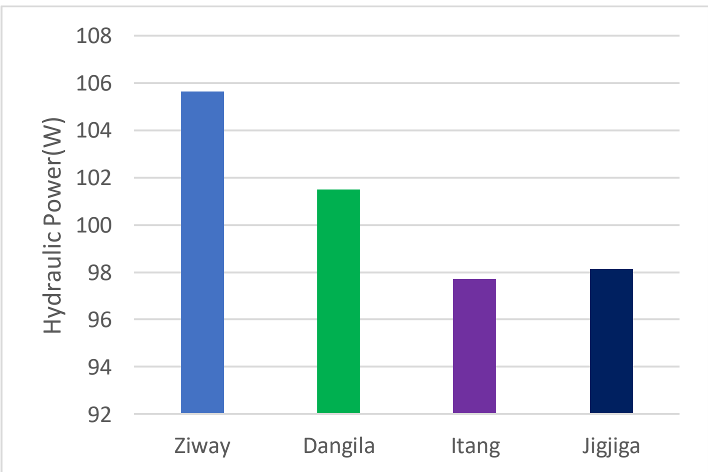

Figure 12. Hydraulic power of Each Site During the March Season

10.57647/ijeee. 2024.1502.07

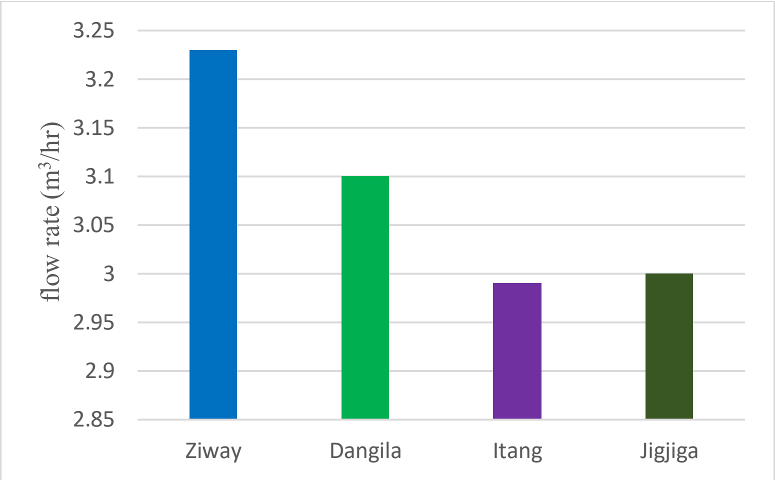

Figure 13. Flow Rate of Each Site During the March Season

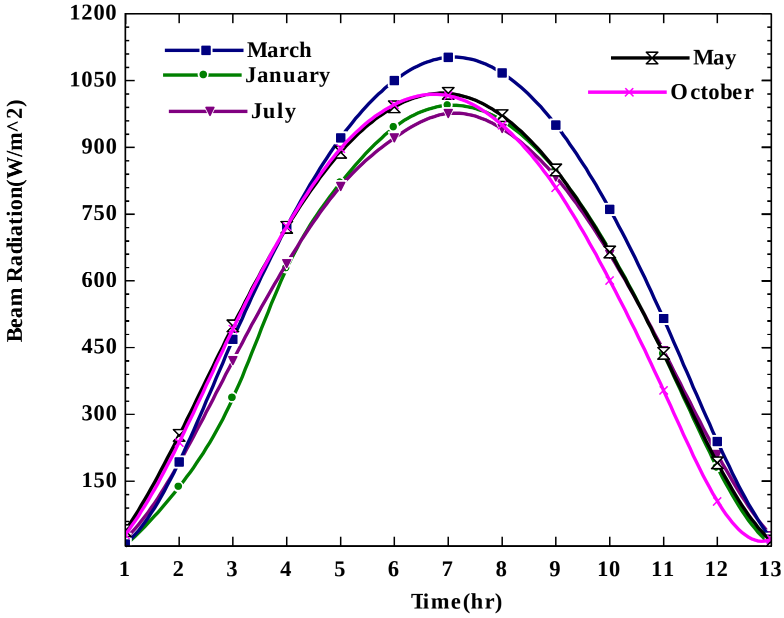

Figure 14. Estimated Monthly Average Hourly Solar Beam Radiation

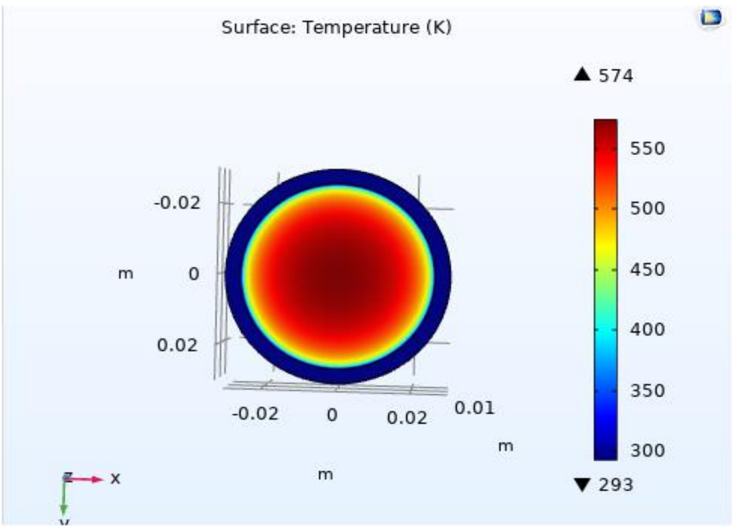

Figure 15. Temperature distribution at the receiver of the concentrator

10.57647/ijeee. 2024.1502.07

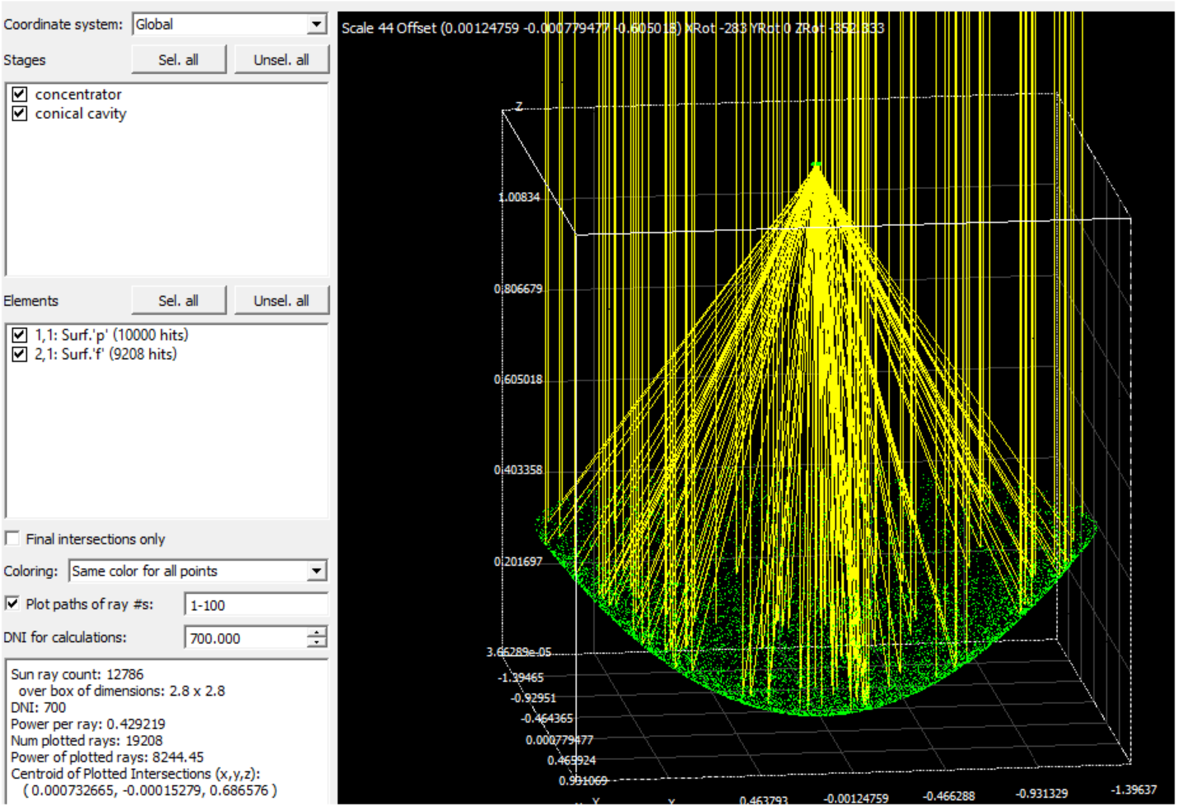

Figure 16. Ray intersection (scatter) plot on the concentrator and absorber

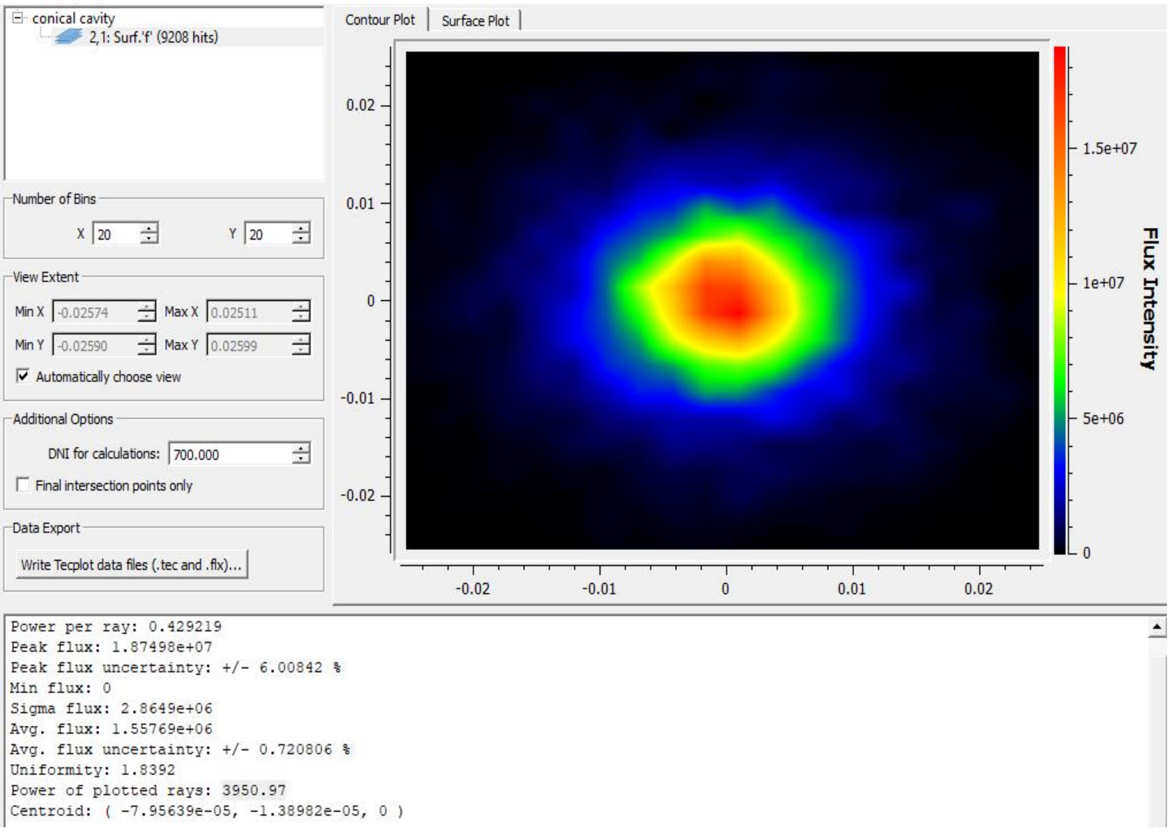

Figure 17. Contour plot (Two-dimensional view) of flux distribution at the focal plane

4.8. Effect of solar heat flux on temperature distribution at the focal plane

Based on solar radiation data obtained from the Ethiopian Meteorological Agency, the average beam radiation at the selected site was estimated to be 700W/m². This irradiance value was input into the Sol Trace simulation software, resulting in a calculated heat flux of approximately 1.5576e+06 W/m² (illustrated in Figure 17). The resulting heat flux was then applied in COMSOL Multiphysics to model the thermal behavior of the receiver, where the inner average surface temperature was found to be 574K. As shown in Figure 17, the temperature distribution gradually decreases from the center to the edge of the absorber.

4.9. Performance of solar dish concentrator

Beam solar radiation is a crucial factor influencing the performance of concentrated solar power systems. The energy transferred to the working fluid in the concentrator's receiver generates steam. Figure 18 shows the variation of beam solar radiation and the outlet working fluid temperature throughout the day on March 16th. As depicted, the beam of solar radiation increases from sunrise, reaching a peak at noon, and then decreases until sunset. Additionally, the shape of the curve is consistent, indicating that the outlet temperature of the working fluid rises linearly with direct solar radiation. At the average beam solar radiation of 700 W/m², the outlet fluid temperature reaches 574 K. Higher solar beam radiation leads to a higher outlet fluid temperature. Figure 20 shows the effect of mass flow rate on the working fluid's outlet temperature at various DNI values, with the ambient temperature held constant at 288 K. As illustrated, the outlet temperature is higher for a given solar radiation intensity at lower mass flow rates. As the mass flow rate increases, the outlet temperature decreases slightly. For example, at a DNI of 1000 W/m², when the mass flow rate increases from 0.002 kg/s to 0.01 kg/s, the outlet temperature drops from 904 K to 424 K.

Figure 21 displays the variation in the working fluid outlet temperature over a sunny day during the irrigation season. The outlet temperature rises from sunrise to midday and then slightly decreases until sunset, reflecting the changes in solar radiation intensity. The temperature fluctuates during the irrigation period, with the highest and lowest temperatures recorded at noon in March (595 K) and July (561 K), respectively. The maximum outlet working fluid temperatures in May, October, and January are estimated at 573 K, 572 K, and 566 K, respectively.

As illustrated in Figure 21, the parabolic dish Stirling engine performs best during midday when solar radiation is strongest, minimizing both heat loss and the heat loss coefficient. Early morning and late evening periods exhibit higher losses, likely due to lower solar intensity and ambient temperature differences, which affect the system's thermal balance.

Figure 22 shows that as the receiver temperature increases, the heat loss increases, and the useful heat decreases. As Figure 23 shows, the heat loss increases consistently as the wind velocity increases. The increased heat loss due to wind reduces the thermal efficiency of the parabolic dish Stirling engine.

As shown in Figure 24, the useful thermal heat in the concentrator's receiver increases with higher solar irradiation. When solar irradiation is varied from 400 to 1000 W/m², the useful thermal heat rises from 2000 W to 5092 W. This shows how solar irradiation impacts thermal performance, with higher DNI resulting in improved thermal performance.

As shown in Figure 25, the exergy and energy efficiency are maximum at noon. This is due to the high solar radiation at that time.

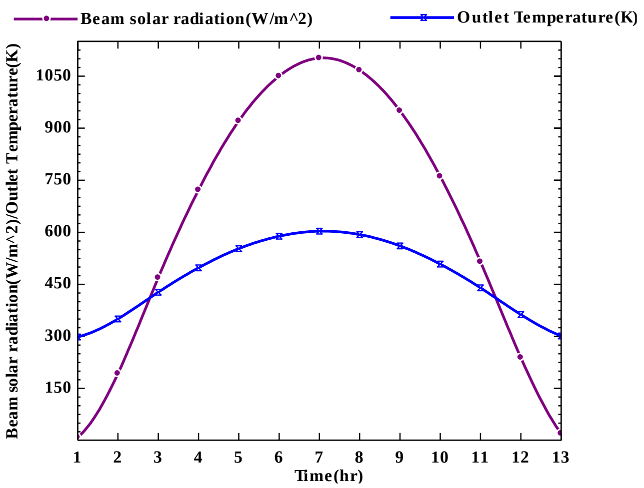

Figure 18. Variation of Beam Solar Radiation and Outlet Temperature of Working Fluid with Time on March 16th

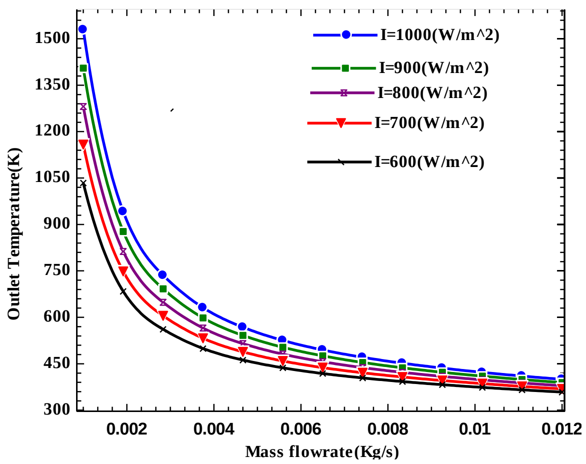

Figure 19. Effect of Working Fluid Mass Flow Rate Temperature under Different Beam Solar Radiation

10.57647/ijeee. 2024.1502.07

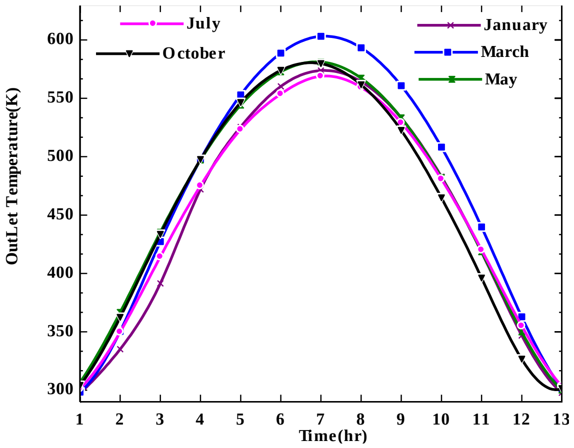

Figure 20. Variation of outlet fluid temperature with time during the day for the selected irrigation season

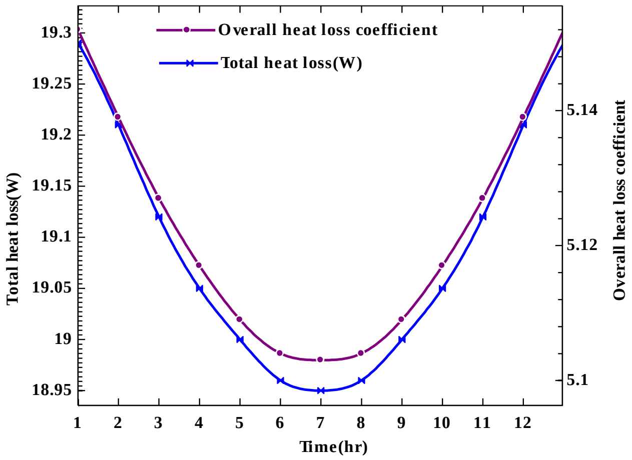

Figure 21. Variation of Heat Loss with Time Over a Day

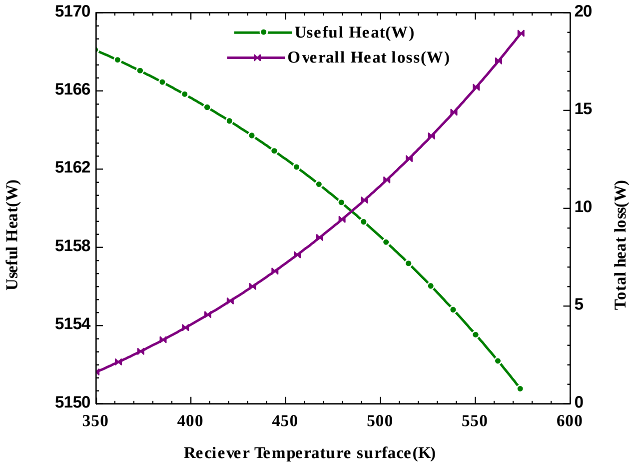

Figure 22. Variation of outlet fluid temperature with time during the day for the selected irrigation season

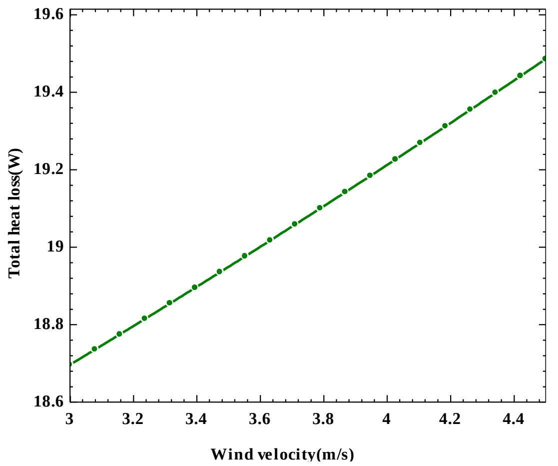

Figure 23. The effect of wind on heat loss

4.10. Analysis of Changes in Thermal Performance and Power Output of a Stirling Engine Over an Irrigation Season

The ideal adiabatic thermal efficiency of the Stirling engine varies each month during the selected irrigation season. Thermal efficiency is influenced by the heat source temperature, with higher temperatures leading to greater efficiency. As shown in Figure 26, the average thermal efficiency peaks in March at 30.62% and is lowest in January at 27.07%. This suggests that both the output power and the pump's required flow rate are dependent on the heat source temperature and the available solar radiation. With higher solar radiation, the heat source temperature increases, allowing the maximum thermal efficiency to be achieved for a given cooler heat exchanger temperature.

The engine's performance is influenced by the heat source temperature, which depends on solar intensity. On a clear day, output power increases steadily from sunrise, peaks at midday, and declines as sunlight diminishes. Maximum power output occurs at midday, with recorded values of 132 W in March, 124.65 W in May, 121.5 W in January, 117 W in October, and 116 W in July, reflecting seasonal variations in solar radiation.

The pump's flow rate is directly influenced by the shaft power of the Stirling engine, with a linear relationship between these parameters. The flow rate follows a diurnal pattern, increasing from sunrise to reach its peak at noontime before gradually declining until sunset, achieving its maximum in March when the pump operates at full capacity to deliver water to the irrigation field.

Based on the hydraulic power of 132 W and the centrifugal pump's efficiency of 85%, the shaft power required to deliver water to the specified location is calculated as 155 W using Eq. (22).

For a given hydraulic pump and a total dynamic head of 12 m. Under these conditions, the estimated pump flow rate is 4.04 m^3/hr. The output power of a Stirling engine influences the pump's flow rate, which depends on the pump's efficiency and static head. Changes in the irrigation period affect the pump's performance. For a given head, higher output power leads to a greater flow rate. If the pump operates for six hours per day each month, it can pump a minimum of 13,113.9 liters per day in July and a maximum of 16,331.28 liters per day in March. The pump's flow rates for January, May, and October are 14520.24 L/day, 14,073.55 L/day, and 14,763 L/day, respectively.

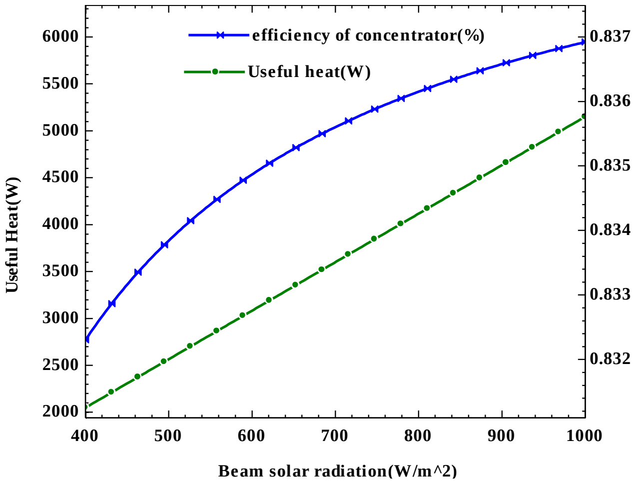

Figure 24. Effect of Beam Solar Radiation (DNI) on the useful heat and instantaneous thermal efficiency of the concentrator

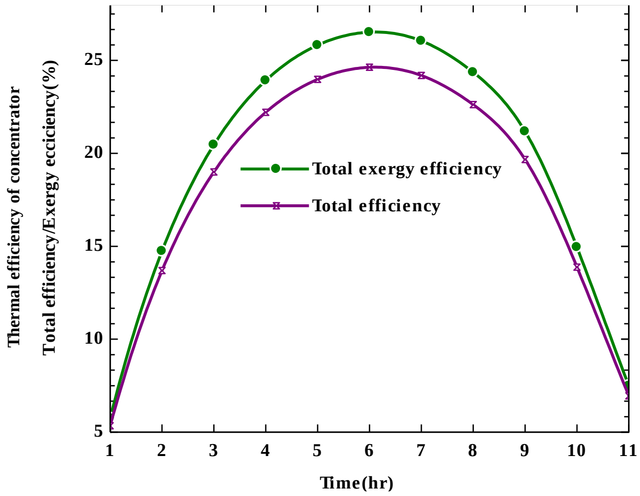

Figure 25. Exergy and energy efficiency with time variation

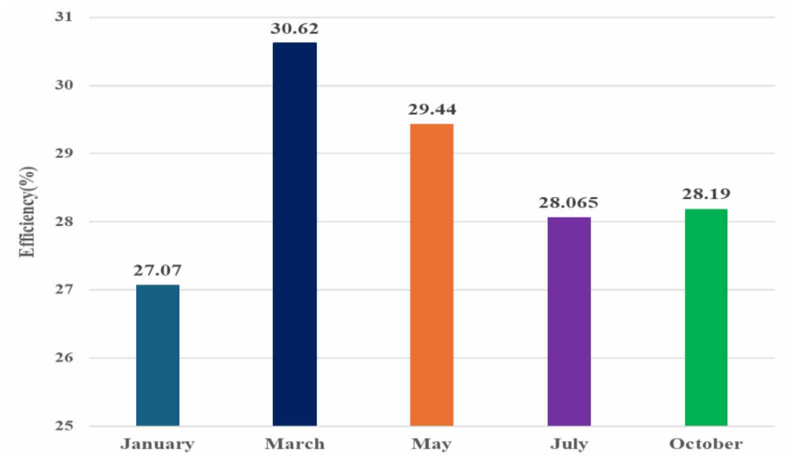

Figure 26. Ideal adiabatic thermal efficiency of the Stirling for selected irrigation periods

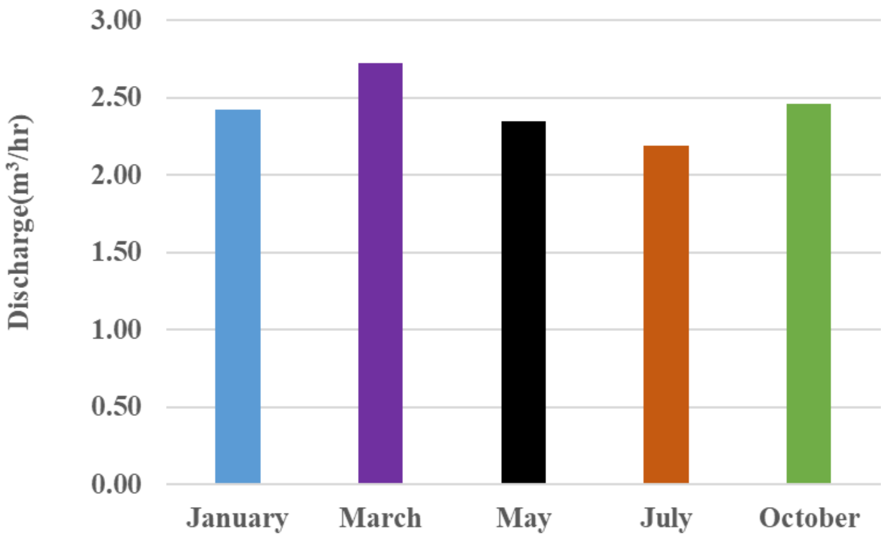

Figure 29. Daily Average flow rate of the pump for the selected irrigation period

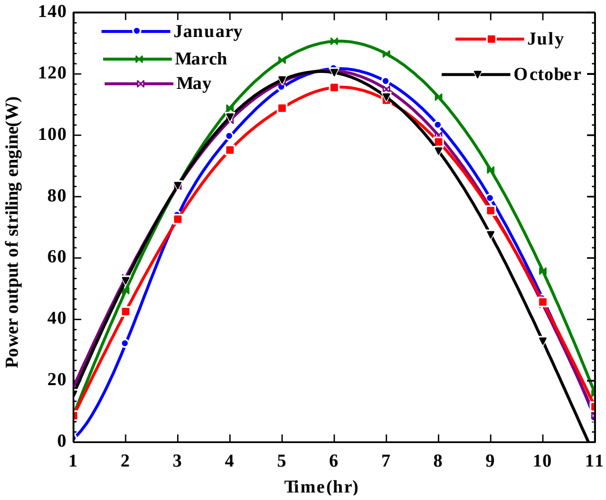

Figure 27. Variation of Stirling engine output power during a time of day for a given irrigation season

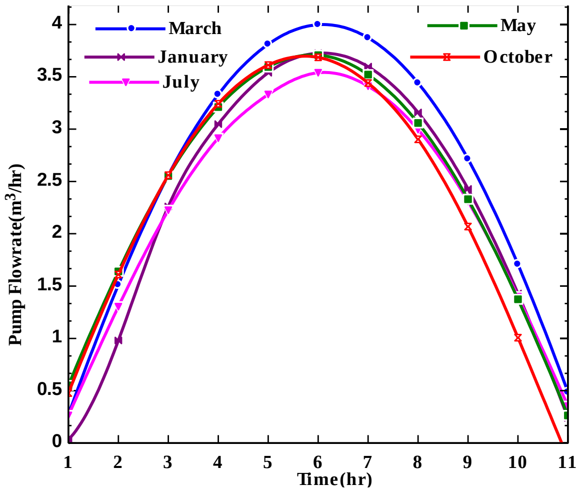

Figure 28 Variation of pump flow rate during a time of day for a given irrigation season

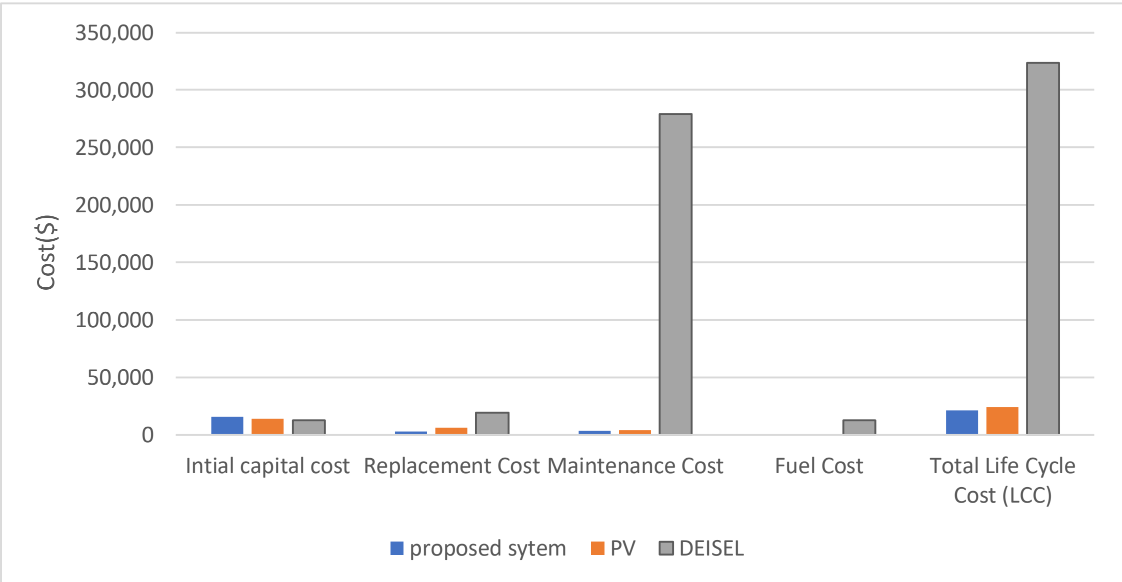

Figure 30. Life cycle cost comparison of the proposed system with the PV and diesel water pumping system.

4.11. Life-Cycle Cost Analysis of Parabolic Dish Stirling, PV, and Diesel-Based Irrigation System

To analyze the cost of a parabolic dish concentrator compared to PV solar panels and diesel generators for an irrigation system, data for PV solar panels and diesel generators were obtained from the Oromia Water and Energy Bureau. The cost of the parabolic dish concentrator, on the other hand, was sourced from global market analyses and research findings, particularly the study reported by [42]. The Oromia Water and Energy Bureau are a significant organization involved in both local and international procurement of PV solar panels and diesel generators for water pumping applications. Their data provides a reliable benchmark for evaluating the cost-effectiveness of these technologies in real-world applications. The projected lifespan of the system is assumed to be 25 years, with an interest rate of 5% applied in all calculations. The daily energy requirement for irrigating 10 hectares of farmland is 2835 W. The replacement costs for the pump and control system are $1964.5 and $798.1, respectively.

4.12. Comparative LCC analysis of the proposed model with PV pumping and diesel system

Twelve PV solar panels (250W each) are considered sufficient to meet the demand for irrigating 10 hectares of farmland. The total initial capital cost of the PV panels is $8,900, according to the Oromia Water and Energy Bureau. The cost of the solar PV pump is $3,400, which is replaced every seven years, and the pump controller costs $1,630, replaced every ten years. The maintenance cost of the solar PV system is assumed to be 2% of the initial capital cost. The replacement costs for the PV pump after seven, fourteen, and twenty-one years are $2,416.32, $1,717.23, and $1,220.40, respectively. For the pump controller, the replacement cost after ten years is $1,000.68. Two 1.5 kW standard generators are used to supply the same load, each costing $2.5 per peak watt and having a lifespan of 10 years. The initial cost of a diesel generator is $7,500, and it consumes 7 liters of diesel fuel per hour, according to the Oromia Water and Energy Bureau. The generator is assumed to operate for six hours per day to meet the irrigation system's needs. The maintenance cost for the diesel generator system is estimated at 15% of the initial cost. The current price of diesel fuel in Ethiopia is $0.728 per liter.

The replacement costs for the diesel pump at five, ten, fifteen, and twenty years are $3,134.10, $2,455.65, $1,924.07, and $1,501.56, respectively. For the pump controller, the replacement costs at five, ten, fifteen, and twenty years are $940.23, $736.70, $577.22, and $452.27, respectively. Since the diesel generator's lifetime is assumed to be ten years, the replacement cost, considering the time value of money, is $4,604.35.

Table 7. Life cycle cost analysis of dish concentrator and thermal Stirling pump

Component	Initial capital cost ($)	Present worth ($
Solar dish concentrator	7000	7000
Stirling engine	4000	4000
Centrifugal pump	3200	3200
Centrifugal pump 10 years	3200	1964.5
Controlling system	1300	1300
Controlling system for 10 years	1300	798.1
Annual maintenance (1% CC)		3100.00
	LCC	21,362.60

Table 8. Life cycle cost analysis of PV solar pumping

Component	Initial capital cost ($)	Present worth ($)
PV Solar Array	8900	8900
Submersible Pump	3400	3400
Submersible Pump 7-year	3400	2416.32
Submersible Pump 14-year	3400	1717.23
Submersible Pump 21 years	3400	1220.40
Pump Controller	1630	1630
Pump controller 10 years	1630	1000.68
Annual maintenance (2% CC)	278.6	3926.573
	LCC	24211.203

Table 9. Life cycle cost analysis of diesel generator pumping system

Component	Initial capital cost ($)	Present worth ($
Diesel Generator	7500	7500
Diesel generator 10-year	7500	4604.35
Diesel generator 20 years	7500	2826.67
Pump	4000	4000
Pump 5 years	4000	3134.1
Pump 10 years	4000	2455.65
Pump 15 years	4000	1924.07
Pump 20 years	4000	1501.56
Pump controller	1200	1200
Pump controller 5-year	1200	940.23
Pump controller 10-year	1200	736.7
Pump controller 15 years	1200	577.22
Pump controller 20-year	1200	452.27
Fuel cost	11160.24	279006
Annual maintenance cost	500	12500
	LCC	323,358.82

The comparison of life cycle costs among the systems demonstrates that the proposed system is more viable and feasible compared to PV and diesel generator systems. As shown in Figure 13, the diesel system has the lowest upfront cost; however, it is less cost-effective over its lifetime due to high operational expenses. Maintenance costs are negligible for both the proposed and PV systems compared to the diesel system, which bears a substantial maintenance burden. Additionally, both the proposed and PV systems outperform the diesel system in operational efficiency as they incur no fuel costs. The proposed system emerges as the most cost-effective and sustainable option, featuring the lowest total life cycle cost (LCC), no fuel costs, and minimal maintenance requirements. Therefore, it is considered the most economically viable choice and is highly recommended for smallholder farmers in Ethiopia's rural areas to support small-scale irrigation.

5. FutureWork

Future research should aim to enhance the application and sustainability of solar dish–Stirling engine systems for irrigation using practical and integrated approaches. Studies could focus on improving heat transfer in the receiver, combining the system with other renewable energy sources like solar PV or wind for a stable power supply, and scaling up for medium- and large-scale irrigation to assess economic feasibility and performance in diverse conditions. Promoting local manufacturing, operation, and maintenance can reduce costs, improve accessibility, and encourage adoption in rural communities. Training local technicians will strengthen technical capacity, reduce reliance on imported technology, and foster innovation. Collaboration among research institutions, universities, and small-scale manufacturers can accelerate system development and dissemination while creating economic opportunities. Future work should also explore advanced materials for receivers and reflectors, integrate automated solar tracking, carefully select sites with high solar potential, and conduct field testing to validate long-term reliability, water delivery, and maintenance needs.

6. Conclusion

The results of this study demonstrate that a solar dish concentrator integrated with a Stirling engine and a conical cavity receiver can provide a reliable, efficient, and sustainable solution for irrigation in regions with water scarcity and high energy costs. The system, with a concentrator efficiency **of 83.69%** and a Stirling engine efficiency of **39.01%,** can deliver a daily water output of **24,240 liters**, sufficient to irrigate **approximately 10 hec**tares of farmland, thereby supporting smallholder agriculture and enhancing resilience against drought and rainfall variability. The conical cavity receiver improves heat flux distribution, reduces thermal stresses, and enhances overall system efficiency, while the modular, low-maintenance parabolic dish–Stirling engine offers a clean, flexible, and durable energy source. Compared to diesel-based irrigation, the solar system significantly reduces operational costs, greenhouse gas emissions, and environmental pollution, promoting economic, environmental, and social benefits. Moreover, the technology is suitable for local fabrication, capacity building, and broader technology transfer. Overall, this study confirms that the solar dish–Stirling system with a conical cavity receiver is a technically feasible, economically viable, and environmentally sustainable solution for smallholder irrigation, offering a pathway toward energy-secure, climate-resilient, and sustainable agricultural development.

Acknowledgment

The authors would like to thank the Jimma Institute of Technology Center of Excellence, Jimma University, for their support during the work on this research.

Authors Contribution
All authors have contributed equally to prepare the paper.

Availability of data and materials
The data that support the findings of this study are available from the corresponding author, upon reasonable request.

Conflict of interests
The authors declare that they have no known competing financial interests or personal relationships that could have appeared to influence the work reported in this paper.

Reference

1. A.-R. Bawa, A. K. Sunnu, and E. A. Sarsah, "Recent advances in solar-powered photovoltaic pumping systems for drip irrigation," *IRASD J. Energy Environ.*, vol. 4, no. 2, pp. 112–132, 2023.
2. D. Vallejo-Gomez, M. Osorio, and C. A. Hincapie, "Smart irrigation systems in agriculture: A systematic review," *Agronomy*, vol. 13, no. 2, p. 342, 2023.
3. P. E. Campana, I. Papic, S. Jakobsson, and J. Yan, "Photovoltaic water pumping systems for irrigation: principles and advances," *Sol. Energy Adv. Agric. Food Prod. Syst.*, pp. 113–157, 2022.
4. U. Ahmad, A. Alvino, and S. Marino, "Solar fertigation: A sustainable and smart IoT-based irrigation and fertilization system for efficient water and nutrient management," *Agronomy*, vol. 12, no. 5, p. 1012, 2022.
5. M. F. Alam *et al.*, "Energy consumption as a proxy to estimate groundwater abstraction in irrigation," *Groundw. Sustain. Dev.*, vol. 23, p. 101035, 2023.
6. A. Ashraf and K. Jamil, "Solar-powered irrigation system as a nature-based solution for sustaining agricultural water management in the Upper Indus Basin," *Nat.-Based Solut.*, vol. 2, p. 100026, 2022.
7. M. Bouzguenda, S. Rajamohamed, M. H. Shwehdi, and A. Aldalbahi, "Solar-powered smart irrigation system based on low-cost wireless network: A senior design project experience," *Int. J. Electr. Eng. Educ.*, vol. 59, no. 4, pp. 404–417, Oct. 2022. Doi: https://doi.org/10.1177/0020720919860414
8. K. Obaideen *et al.*, "Solar energy: Applications, trends analysis, bibliometric analysis and research contribution to sustainable development goals (SDGs)," *Sustainability*, vol. 15, no. 2, p. 1418, 2023.

9. C. Heracleous, A. Michael, A. Savvides, and C. Hayles, “A methodology to assess energy-demand savings and cost-effectiveness of adaptation measures in educational buildings in the warm Mediterranean region,” *Energy Rep.*, vol. 8, pp. 5472–5486, 2022.
10. A. Bathaei and D. Štreimikienė, “Renewable energy and sustainable agriculture: Review of indicators,” *Sustainability*, vol. 15, no. 19, p. 14307, 2023.
11. G. Ferruzzi *et al.*, “Concentrating solar power: the state of the art, research gaps and future perspectives,” *Energies*, vol. 16, no. 24, p. 8082, 2023.
12. I. Kyeyune and J. Wanyama, “Design optimization of communal solar powered irrigation system,” *Afr. J. Agric. Res.*, vol. 19, no. 3, pp. 272–286, 2023.
13. A. F. M. Saleh, M. Al Asif, and N. R. Naomi, “A Multi-Criteria Analysis on Solar and Traditional Technologies in Irrigation Development,” *J. Eng. Sci.*, vol. 13, no. 2, pp. 101–110, 2022.
14. S. M. Wazed, B. R. Hughes, D. O’Connor, and J. K. Calautit, “Solar-driven irrigation systems for remote rural farms,” *Energy Procedia*, vol. 142, pp. 184–191, 2017.
15. M. Al-Nimr, S. A. Khashan, and H. Al-Oqla, “Novel techniques to enhance the performance of Stirling engines integrated with solar systems,” *Renew. Energy*, vol. 202, pp. 894–906, 2023.
16. B. Terang and D. C. Baruah, “Techno-economic and environmental assessment of solar photovoltaic, diesel, and electric water pumps for irrigation in Assam, India,” *Energy Policy*, vol. 183, p. 113807, 2023.
17. S. M. Wazed, B. R. Hughes, D. O’Connor, and J. K. Calautit, “A review of sustainable solar irrigation systems for Sub-Saharan Africa,” *Renew. Sustain. Energy Rev.*, vol. 81, pp. 1206–1225, 2018.
18. K. N. Tiwari, M. V. Hadole, and P. Bajpai, “Solar Photovoltaic Pump-operated Micro-irrigation Systems: A Comprehensive Review,” *J. Agric. Eng.*, vol. 59, no. 4, pp. 369–385, 2022.
19. M. Rostami, E. Assareh, R. Moltames, and T. Jafarinejad, “Thermo-economic analysis and multi-objective optimization of a solar dish Stirling engine,” *Energy Sources Part Recovery Util. Environ. Eff.*, vol. 43, no. 22, pp. 2861–2877, Nov. 2021 Doi: https://doi.org/10.1080/15567036.2020.1834027
20. B. Ali, “Comparative assessment of the feasibility for solar irrigation pumps in Sudan,” *Renew. Sustain. Energy Rev.*, vol. 81, pp. 413–420, 2018.
21. S. Agrawal and A. Jain, “Sustainable deployment of solar irrigation pumps: Key determinants and strategies,” *WIREs Energy Environ.*, vol. 8, no. 2, p. e325, Mar. 2019, Doi: https://doi.org/10.1002/wene 325
22. Y. W. Wong and K. Sumathy, “Solar thermal water pumping systems: a review,” *Renew. Sustain. Energy Rev.*, vol.. 3, no. 2–3, pp. 185–217, 1999.
23. M. A. Biberci, “Techno-economic analysis of a solar-powered agricultural irrigation system using PV* Sol software: A case study in Konya,” *Int. J. Agric. Environ. Food Sci.*, vol. 7, no. 1, pp. 156–162, 2023
24. S. K. Vishnu and R. Senthil, “Experimental performance and economic analysis of finned solar receiver for parabolic dish solar collector,” *Heliyon*, vol. 9, no. 11, p. e21236, Nov. 2023. Doi: https://doi.org/10.1016/j.heliyon.2023.e21236
25. N. Ghazouani, A. A. El-Bary, G. E. Hassan, N. Becheikh, A. Bawadekji, and M. M. Elewa, “Solar desalination by humidification–dehumidification: A review,” *Water*, vol. 14, no. 21, p. 3424, 2022
26. A. Alhawsawi, M. E. Zayed, E. Moustafa, E. Banoqitah, and A. H. Elsheikh, “Hybridizing solar dish Stirling power system with single-effect desalination for sustainable electricity and freshwater co-generation: Mathematical modeling and performance evaluation,” *Case Stud. Therm. Eng.*, vol. 45, p. 102997, 2023.
27. M. I. Al-Amayreh, A. Alahmer, and A. Manasrah, “A novel parabolic solar dish design for a hybrid solar lighting-thermal applications,” *Energy Rep.*, vol. 6, pp. 1136–1143, 2020.
28. M. M. Aboelmaaref *et al.*, “Research on solar dish/Stirling engine driven adsorption-based desalination system for simultaneous co-generation of electricity and freshwater: Numerical investigation,” *Case Stud. Therm. Eng.*, vol. 47, p. 103044, 2023.
29. G. Falchetta, F. Semeria, M. Tuninetti, V. Giordano, S. Pachauri, and E. Byers, “Solar irrigation in sub-Saharan Africa: economic feasibility and development potential,” *Environ. Res. Lett.*, vol. 18, no. 9, p. 094044, 2023.
30. F. Hussain *et al.*, “Solar irrigation potential, key issues and challenges in Pakistan,” *Water*, vol. 15, no. 9, p. 1727, 2023.
31. S. K. Vishnu and R. Senthil, “Experimental performance evaluation of a solar parabolic dish collector using spiral flow path receiver,” *Appl. Therm. Eng.*, vol. 231, p. 120979, 2023.
32. G. Panse-Aglave and Q. Hassan, “A review paper on energy harvesting in arid and semi-arid regions via PV cells on irrigation canals,” *Mater. Today Proc.*, vol. 69, pp. 582–586, 2022.
33. M. Rostami, E. Assareh, R. Moltames, and T. Jafarinejad, “Thermo-economic analysis and multi-objective optimization of a solar dish Stirling engine,” *Energy Sources Part Recovery Util. Environ. Eff.*, vol. 43, no. 22, pp. 2861–2877, Nov. 2021. Doi: https://doi.org/10.1080/15567036.2020.1834027
34. H. Allouhi, A. Allouhi, and A. Jamil, “Multi-objective optimization of a CSP-based dish Stirling field layout using Genetic Algorithm and TOPSIS method: Case studies in Ouarzazate and Madrid,” *Energy Convers. Manag.*, vol. 254, p. 115220, 2022.
35. P. Heller, *The performance of concentrated solar power (CSP) systems: analysis, measurement and assessment*. Woodhead Publishing, 2017.
36. V. Thirunavukkarasu, V. U. Nair, K. Tiwari, and M. Cheralathan, “Experimental investigation on thermal performance of cavity receiver integrated with short-term thermal energy storage for a solar parabolic dish concentrator,” *J. Therm. Anal. Calorim.*, vol. 147, no. 1, pp. 741–752, Jan. 2022. Doi: https://doi.org/10.1007/s10973-020-10387-6
37. M. E. Zayed, J. Zhao, A. H. Elsheikh, W. Li, and M. Abd Elaziz, “Optimal design parameters and performance optimization of thermodynamically balanced dish/Stirling concentrated solar power system using multi-objective particle swarm optimization,” *Appl. Therm. Eng.*, vol. 178, p. 115539, 2020.
38. M. E. Zayed, J. Zhao, A. H. Elsheikh, W. Li, S. Sadek, and M. M. Aboelmaaref, “A comprehensive review on Dish/Stirling concentrated solar power systems: Design, optical and geometrical analyses, thermal performance assessment, and applications,” *J. Clean. Prod.*, vol. 283, p. 124664, 2021.
39. A. Basem, M. Moawed, M. H. Abbood, and W. M. El-Maghlany, “The energy and exergy analysis of a combined parabolic solar dish–steam power plant,” *Renew. Energy Focus*, vol. 41, pp. 55–68, 2022.
40. O. M. Elmardi Suleiman, “Performance and Design Optimization of Solar Powered Stirling Engine Using Genetic Algorithm,” *Glob. J. Eng. Sci.*, vol. 1, no. 1, Sep. 2018. Doi: https://doi.org/10.33552/GJES.2018.01.000501
41. F. Aksoy, H. Solmaz, M. Arslan, E. Yılmaz, D. İpci, and A. Calam, “Effects of the regenerator on engine performance of a rhombic drive beta type stirling engine,” *Energy Sources Part Recovery Util. Environ. Eff.*, pp. 1–9, Apr. 2021 Doi: https://doi.org/10.1080/15567036.2021.1912853

42. E. A. Bekele and V. R. Ancha, “Transient performance prediction of solar dish concentrator integrated with stirling and TEG for small-scale irrigation system: A case of Ethiopia,” *Heliyon*, vol. 8, no. 9, p. e10629, Sep. 2022. Doi: https://doi.org/10.1016/j.heliyon.2022.e10629
43. J. Liu, Y. Shen, G. Zhou, D.-L. Liu, Q. Yu, and J. Du, “Calibrating the Ångström–Prescott Model with Solar Radiation Data Collected over Long and Short Periods of Time over the Tibetan Plateau,” *Energies*, vol. 16, no. 20, p. 7093, 2023.
44. W. Zhu *et al.*, “Estimating sunshine duration using hourly total cloud amount data from a geostationary meteorological satellite,” *Atmosphere*, vol. 11, no. 1, p. 26, 2019.
45. S. A. Mousavi Maleki, H. Hizam, and C. Gomes, “Estimation of hourly, daily, and monthly global solar radiation on inclined surfaces: Models re-visited,” *Energies*, vol. 10, no. 1, p. 134, 2017.
46. M. B. Moisa *et al.*, “Evaluation of the groundwater recharge potential zone by using GIS and remote sensing in Ziway Abijata sub-basin, Central Rift Valley of Ethiopia,” *Water Supply*, vol. 23, no. 8, pp. 3416–3431, Aug. 2023. Doi: https://doi.org/10.2166/ws.. 2023.183
47. Z. Shelemew, D. Hussen, A. Ambomsa, and A. Jelde, “Identification, Characterization and Mapping of Potential Irrigable Areas in Ziway Micro Watershed,” *Int. J. Econ. Energy Environ.*, vol. 7, no. 3, pp. 62–66, 2022.
48. M. B. Moisa *et al.*, “Evaluation of the groundwater recharge potential zone by using GIS and remote sensing in Ziway Abijata sub-basin, Central Rift Valley of Ethiopia,” *Water Supply*, vol. 23, no. 8, pp. 3416–3431, 2023.
49. D. G. Eshete *et al.*, “Evaluation of Shallow Ground Water Recharge and Its Potential for Dry Season Irrigation at Brante Watershed, Dangila, Ethiopia,” in *Advances of Science and Technology*, vol. 308, N. G. Habtu, D. W. Ayele, S. W. Fanta, B. T. Admasu, and M. A. Bitew, Eds., in Lecture Notes of the Institute for Computer Sciences, Social Informatics and Telecommunications Engineering, vol. 308. , Cham: Springer International Publishing, 2020, pp. 148–168. Doi: https://doi.org/10.1007/978-3-030-43690-2_11
50. T. Ayenew, M. GebreEgziabher, S. Kebede, and S. Mamo, “Integrated assessment of hydrogeology and water quality for groundwater-based irrigation development in the Raya Valley, northern Ethiopia,” *Water Int.*, vol. 38, no. 4, pp. 480–492, Jul. 2013. Doi: https://doi.org/10.1080/02508060.2013.821640
51. Y. Zhang *et al.*, “Characterization of soil salinization and its driving factors in a typical irrigation area of Northwest China,” *Sci. Total Environ.*, vol. 837, p. 155808, 2022.
52. T. D. Mengistu *et al.*, “Challenges and prospects of advancing groundwater research in Ethiopian aquifers: A review,” *Sustainability*, vol. 13, no. 20, p. 11500, 2021.
53. Z. Stevanović and S. Kebede, “Jurassic Carbonate Aquifer—The Most Valuable Fresh Water Resource at the Horn of Africa,” in *Eurokarst 2018, Besançon*, C. Bertrand, S. Denimal, M. Steinmann, and P. Renard, Eds., in Advances in Karst Science. , Cham: Springer International Publishing, 2020, pp. 213–221. Doi: https://doi.org/10.1007/978-3-030-14015-1_24
54. S. Godfrey, G. Hailemichael, and C. Serele, “Deep groundwater as an alternative source of water in the Ogaden Jesoma sandstone aquifers of Somali region, Ethiopia,” *Water*, vol. 11, no. 8, p. 1735, 2019.
55. D. BÜYÜKTAŞ, “WATER RESOURCE and IRRIGATION in SOMALIA: A REVIEW Yasin Mohamed IBRAHİM Cihan KARACA,” *Curr. Res. Agric. For. Aquac. Sci.*, p. 35.
56. B. A. Yifru, D. B. Mitiku, M. B. Tolera, S. W. Chang, and I.-M. Chung, “Groundwater potential mapping using SWAT and GIS-based multi-criteria decision analysis,” *KSCE J. Civ. Eng.*, vol. 24, no. 8, pp. 2546–2559, 2020.
57. M. N. A. Talib, M. Ahmed, M. M. Naseer, B. Slusarczyk, and J. Popp, “The long-run impacts of temperature and rainfall on agricultural growth in Sub-Saharan Africa,” *Sustainability*, vol. 13, no. 2, p. 595, 2021.
58. M. M. Alemu and F. Y. Desta, “Seasonal rainfall and crop productivity in South West Ethiopia: Preliminary analysis for recent climate,” *Int. J. Water Resour. Environ. Eng.*, vol.. 9, no. 10, pp. 211–217, 2017.
59. Z. I. A. ALhsani and R. K. AL-Dulaimi, “Experimental analysis of solar dish concentrators with cylindrical, oval, and conical cavity receivers,” *Int. J. Renew. Energy Res. IJRER*, vol. 10, no. 2, pp. 591–600, 2020.
60. H. Liu, J. Deng, Y. Guan, and L. Wang, “Study of Heat Flux Density of Dish Solar Cavity Heat Absorber,” *Energies*, vol. 15, no. 21, p. 7946, Oct. 2022. Doi: https://doi.org/10.3390/en15217946
61. S. Guarino, A. Buscemi, A. Messineo, and V. Lo Brano, “Energy and environmental assessment of a hybrid dish-stirling concentrating solar power plant,” *Sustainability*, vol. 14, no. 10, p. 6098, 2022.
62. V. Siva Reddy, S. C. Kaushik, and S. K. Tyagi, “Exergetic analysis and performance evaluation of parabolic dish Stirling engine solar power plant: Parabolic dish Stirling engine solar power plant,” *Int. J. Energy Res.*, vol. 37, no. 11, pp. 1287–1301, Sep. 2013. Doi: https://doi.org/10.1002/er.2926
63. A. A. Cuadri, J. E. Martín-Alfonso, and J. Urbano, “A teaching methodology based on Mathcad for improving the calculation of pumping power,” *Educ. Chem. Eng.*, vol. 28, pp. 68–78, 2019.
64. J. Benavides, E. Hernández-Plaza, L. Mateos, and E. Fereres, “A global analysis of irrigation scheme water supplies in relation to requirements,” *Agric. Water Manag.*, vol. 243, p. 106457, 2021.
65. A. Dénarié, M. Aprile, and M. Motta, “Dynamical modelling and experimental validation of a fast and accurate district heating thermo-hydraulic modular simulation tool,” *Energy*, vol. 282, p. 128397, 2023.
66. G. M. D. Putra, D. A. Setiawati, and S. Sumarjan, “Water Balance Analysis In Pijenan Bantul Irrigation Area,” *J. Agrotek Ummat*, vol. 5, no. 1, pp. 37–45, 2018.
67. Z. Girma, “Techno-economic analysis of photovoltaic pumping system for rural water supply in Ethiopia,” *Int. J. Sustain. Energy*, vol. 36, no. 3, pp. 277–295, Mar. 2017. Doi: https://doi.org/10.1080/14786451.2015.1017498
68. Z. I. A. ALhsani and R. K. AL-Dulaimi, “Experimental analysis of solar dish concentrators with cylindrical, oval, and conical cavity receivers,” *Int. J. Renew. Energy Res. IJRER*, vol. 10, no. 2, pp. 591–600, 2020.
69. A. M. Daabo, S. Mahmoud, and R. K. Al-Dadah, “The optical efficiency of three different geometries of a small-scale cavity receiver for concentrated solar applications,” *Appl. Energy*, vol. 179, pp. 1081–1096, 2016.
70. P. Puech and V. Tishkova, “Thermodynamic analysis of a Stirling engine including regenerator dead volume,” *Renew. Energy*, vol. 36, no. 2, pp. 872–878, 2011.
71. M. E. Zayed, J. Zhao, and A. E.-N. Kabeel, “Dish/Stirling Concentrated Solar Power Plant for Smart Grid Power Generation: Field Testing, Operational Experience, and Dynamic Performance Modeling,” *Delta Univ. Sci. J.*, vol. 6, no. 1, pp. 211–224, 2023.
72. A. A. Sabziparvar, R. Mousavi, S. Marofi, N. A. Ebrahimipak, and M. Heidari, “An Improved Estimation of the Angstrom–Prescott Radiation Coefficients for the FAO56 Penman–Monteith Evapotranspiration Method,” *Water Resour. Manag.*, vol. 27, no. 8, pp. 2839–2854, Jun. 2013. Doi: https://doi.org/10.1007/s11269-013-0318-z